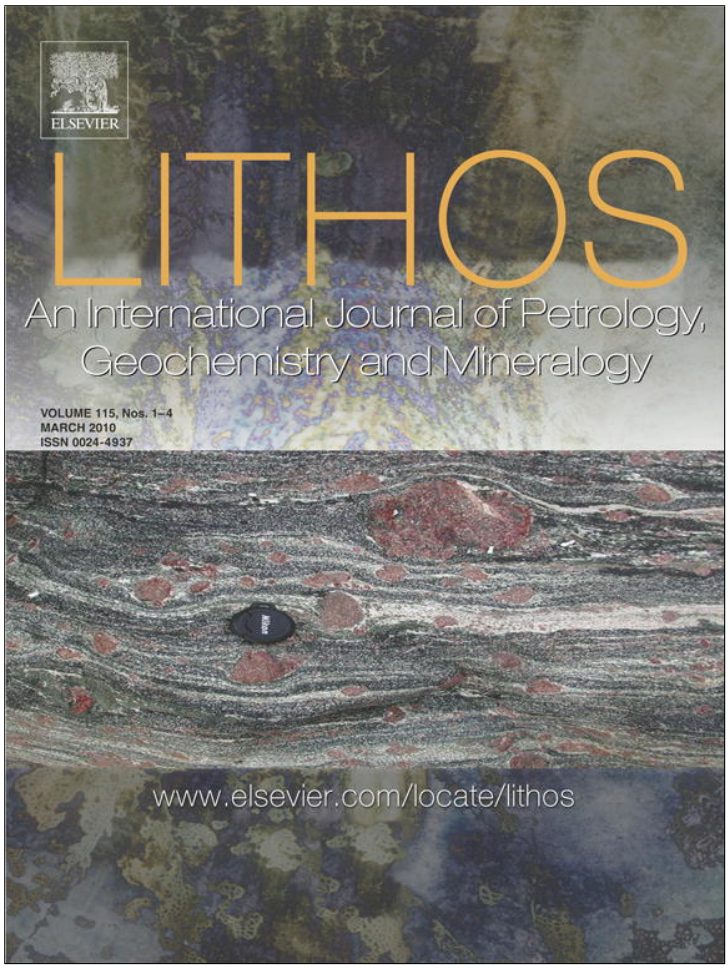

Lithos 115 (2010) 65–81

Contents lists available at ScienceDirect

Lithos

journal homepage: www.elsevier.com/locate/lithos

Fault controlled Carboniferous A-type magmatism in the proto-Andean foreland (Sierras Pampeanas, Argentina): Geochemical constraints and petrogenesis

Juan A. Dahlquist [a,b,*], Pablo H. Alasino [b,c], G. Nelson Eby [d], Carmen Galindo [e], César Casquet [e]

[a] CICTERRA-CONICET-UNC, Av. Vélez Sarsfield 1611, Pab. Geol., X5016CGA-Córdoba, Argentina
[b] UNLaR, Av. Dr. Rene Favaloro, 5300-La Rioja, Argentina
[c] CRILAR-CONICET, Anillaco Entre Ríos y Mendoza, (5301), Anillaco, La Rioja, Argentina
[d] Department of Environmental, Earth, and Atmospheric Sciences, University of Massachusetts, Lowell, Massachusetts 01854, USA
[e] Departamento de Petrología y Geoquímica, Universidad Complutense, 28040 Madrid, Spain

ARTICLE INFO

Article history:
Received 30 April 2009
Accepted 12 November 2009
Available online 26 November 2009

Keywords:
Early Carboniferous
A-type magmatism
Geochemistry
Biotite chemistry
Sr–Nd isotopes
Shear zones

ABSTRACT

The intrusion of granitoids into the Eastern Sierras Pampeanas in the Early Carboniferous took place after a long period of mainly compressional deformation that included the Famatinian (Ordovician) and Achalian (Devonian) orogenies. These granitoids occur as small scattered plutons emplaced in a dominant extensional setting, within older metamorphic and igneous rocks, and many of them are arranged along a reactivated large shear zone. A set of 46 samples from different granitic rocks: Huaco granitic complex, San Blas pluton, and the La Chinchilla stock from the Sierra de Velasco, Zapata granitic complex from Sierra de Zapata, and the Los Árboles pluton from Sierra de Fiambalá, display high and restricted SiO_2 contents between 69.2 and 76.4 wt.%. On both $FeO/(FeO+MgO)$ vs. SiO_2 and $[(Na_2O+K_2O)-CaO]$ vs. SiO_2 plots the samples plot in the ferroan and alkaline-calcic to calco-alkaline fields ($FeO/(FeO+MgO)=0.88–1.0\%$;$[(Na_2O+K_2O)-CaO]=6.3–8.3\%$), thus showing an A-type granitoid signature. The high concentrations for the High Field Strength Elements (HSFE), such as Y, Nb, Ga, Ta, U, Th, etc. and flat REE patterns showing significant negative Eu anomalies are also typical features of A-type granites. Our petrogenetic model supports progressive fractional crystallization with dominant fractionation of feldspar and a source mineral assemblage enriched in plagioclase. Biotites have distinctive compositions with high FeO/MgO ratios (7.8–61.5), F (360–5610 ppm), and Cl (120–1050 ppm). The FeO/MgO ratios together with the F and Cl content of igneous biotites seem to reflect the nature of their parental host magmas and may be useful in identifying A-type granitoids. The isotopic data (Rb–Sr and Sm–Nd) confirm that the A-type granites represent variable mixtures of asthenospheric mantle and continental crust and different mixtures lead to different subtypes of A-type granite (illustrating the lack of consensus about A-type magma origin). We conclude that prominent shear zones play an important role in providing suitable conduits for ascending asthenospheric material and heat influx in the crust, a hypothesis that is in accord with other recent work on A-type granites.

1. Introduction

The Early Carboniferous granitoids of the Sierras Pampeanas (La Rioja and Catamarca province, Argentina) occur as restricted and scattered outcrops. Most of the granitoids were emplaced along a prominent shear zone (Höckenreiner et al., 2003). The intrusion of these granitoids with an A-type signature (Dahlquist et al., 2006) followed several periods of intense magmatic activity: Middle Cambrian (Pampean Orogen), Early–Middle Ordovician (Famatinian Orogen), and Middle–Upper Devonian (Achalian Orogen). A variety of studies during the past 10 years have improved our understanding of the petrogenesis and timing of the Pampean and Famatinian granitoids, but the late Palaeozoic granites (i.e., Devonian and Carboniferous) emplaced after the metamorphic peak of the Famatinian Orogeny have received relatively little attention. In particular, they were only recently (Dahlquist et al., 2007) recognized as a genetic group representative of a specific magmatic event. The genesis of these granites is not well constrained, and they have been considered as products of a crustal reheating process during a final phase of the Famatinian orogen (e.g. Llambías et al., 1998; Grissom et al., 1998; Höckenreiner et al., 2003; Miller and Söllner, 2005; Grosse et al., 2009) or part of a distinctive orogen called the Achalian (e.g. Sims et al., 1998; Stuart-Smith et al., 1999; Siegesmund et al., 2004; Dahlquist et al., 2006; López de Luchi et al., 2007).

In this paper we present major and trace element data for 46 whole-rock samples, biotite compositions, and Rb–Sr and Sm–Nd isotope data for four Carboniferous large granitic units in the Eastern Sierras Pampeanas of La Rioja and Catamarca provinces.

* Corresponding author. CICTERRA-CONICET-UNC, Av. Vélez Sarsfield 1611, Pab. Geol., X5016CGA-Córdoba, Argentina.
E-mail address: jdahlquist@efn.uncor.edu (J.A. Dahlquist).

0024-4937/$ – see front matter © 2009 Elsevier B.V. All rights reserved.
doi:10.1016/j.lithos.2009.11.006

2. Geological setting

Using geochronological data and association with major orogenic episodes, four main granitoid groups have been recognized in the Eastern Sierras Pampeanas: Gi = Middle Cambrian granites (Pampean), Gii = Early–Middle Ordovician granites (Famatinian), Giii = Middle–Upper Devonian granites, and Giv = Early Carboniferous granites (Sims et al., 1998; Rapela and Pankhurst, 1998; Rapela et al., 1998; Pankhurst et al., 1998, 2000; Dahlquist and Galindo, 2004; Büttner et al., 2005; Miller and Söllner 2005; Dahlquist et al., 2007, 2008; Rapela et al., 2008; Grosse et al., 2009).

The large amount of geochronological data for the Pampean and Famatinian granites reported during the last ten years has improved our knowledge of the timing of these groups, but the Late Paleozoic granites emplaced after the metamorphic peak of the Famatinian Orogeny have received relatively little attention. Sims et al. (1998), Stuart-Smith et al. (1999), and Siegesmund et al. (2004) considered the voluminous Devonian intrusive rocks in the Sierras de Córdoba and the eastern area of the Sierras de San Luis to be associated with Devonian low-grade shear zones, together defining the *Achalian Orogeny* (368 ± 25 Ma U–Pb zircon, Dorais et al. (1997); 393 ± 5 Ma U–Pb SHRIMP zircon, Stuart-Smith et al. (1999); 382 ± 5 Ma Siegesmund et al. (2004); 369 ± 9 Ma Rb/Sr whole-rock, Pinotti et al. (2006); and 379 ± 4 and 369 ± 3 Ma U–Pb SHRIMP zircon; Rapela et al. (2008); Fig. 1). According to this interpretation the Devonian granites, such as the Achala (Sims et al., 1998) and Cerro Áspero batholiths in Sierra de Córdoba (e.g. Pinotti et al., 2002, 2006), and the Las Chacras (Siegesmund et al., 2004) and Renca (Stuart-Smith et al., 1999) batholiths in Sierra de San Luis (Fig. 1), are not post-orogenic intrusions of the Famatinian Orogeny as proposed by Rapela and Pankhurst (1998), but belong to a distinct tectonomagmatic event. In NW Argentina this event produced extensive NNW–SSE trending ductile shear zones, including the *T*Inogasta–*P*ituil–*A*ntinaco (TIPA) shear zone (Höckenreiner et al., 2003, and references therein), that reached amphibolite grade. The Devonian compressional event has also been related either to collision of the Chilenia terrane with the proto-Pacific margin (Sims et al., 1998) or to a final collision between the Famatinian magmatic arc and the Pampean hinterland (Höckenreiner et al., 2003). To be consistent with previous associations between the names of the orogenies and those for the associated granitoids, Dahlquist et al. (2006) referred to all the Devonian and Carboniferous granites as *Achalian granites* (Fig. 1). Recently, these granites have been described by Grosse et al. (2009) as "part of the group of Middle Devonian–Lower Carboniferous granites of Sierras Pampeanas". However, field and geochemical data for the Early Carboniferous granites are indicative of an extensional within-plate setting and noncompressive tectonic regime, not syn-kinematic emplacement as has been invoked for the Devonian granites of Sierras de Córdoba or San Luis (Sims et al., 1998; Stuart-Smith et al., 1999; Siegesmund et al., 2004). Dahlquist et al. (2007) proposed that the Early Carboniferous A-type granites in the Eastern Sierras Pampeanas indicate a new distinctive tectonothermal event, i.e., the *A-type event* of the *Eastern Sierras Pampeanas* (*ATEESP*). This distinct intrusive event preceded the late Carboniferous exhumation of deep metamorphic levels and deposition of the continental sediments of the Paganzo Group. In most cases the Carboniferous granites were emplaced at shallow depth and are dominated by facies with K-feldspar megacrysts. They are relatively small, isolated, sub-circular plutons scattered throughout the Eastern Sierras Pampeanas without any obvious spatial arrangements (although most were emplaced along the reactivated shear zone Fig. 1) or deformation.

3. Field occurrence and petrographic descriptions

Our study was carried out on four representative granitic bodies of Early Carboniferous age which outcrop in the Eastern Sierras Pampeanas of Catamarca and La Rioja provinces (Figs. 1 and 2). These granitic bodies (Los Árboles pluton, San Blas pluton, Zapata granitic complex, Huaco granitic complex) (Figs. 1 and 2) occur along the large TIPA shear zone (Höckenreiner et al., 2003, and references therein). Höckenreiner et al. (2003) have suggested that the U–Pb ages for apatite in the granitic rocks (meta-granodiorite 342 ± 1.8; mylonite 328 ± 3 Ma) of the Sierra de Copacabana (near to the TIPA shear zone, Fig. 1) are consistent with the age of the Carboniferous granites and document a Carboniferous heating process that affected the whole crust.

Petrographic investigations were conducted on 85 samples collected from these four granitic bodies and several smaller granitic bodies — the La Florida pluton and El Salto stock in Sierra de Fiambalá and the La Chinchilla stock in Sierra de Velasco (Figs. 1 and 2). Modal data are plotted in Fig. 3 and reveal a dominant monzogranite composition, transitional to granodiorite and syenogranite (modal data are found in a supplemental electronic data table).

3.1. Los Árboles pluton

The Los Árboles pluton (LAP) (Los Ratones pluton of Grissom et al. (1998)) is an ellipsoidal intrusive body approximately 70 km^2 in area and is located in the central part of the Sierra de Fiambalá. The host rocks are dominantly migmatites-gneisses overprinted by a mylonitic deformation (Grissom et al., 1998; Höckenreiner et al., 2003). The contact of the LAP with the surrounding metamorphic rocks is sharp and intrusive. Metamorphic blocks of meter-scale are found in the intrusive.

Two main facies have been recognized: (1) felsic porphyritic biotite–amphibole granodiorite to monzogranite, found mainly in the western region of the pluton, which has microcline phenocrysts (3 × 1.8 to 1.5 × 0.9 cm) and is typically orange in colour and (2) leucocratic equigranular biotite monzogranite, recognized in the central-northeastern region, which is coarse-grained (~1 cm), equigranular and white in colour. Zircon, monazite, apatite, allanite and oxides are accessory minerals in both igneous facies, although in different proportions. Biotite, containing unidentified radioactive minerals that are surrounded by large, black, pleochroic halos, are common in the leucocratic facies. Poorly aligned microcline phenocrysts define a poorly developed fabric (interpreted as magmatic in origin) which, where measurable, has an orientation of ~340–350°.

A small pluton and a stock, La Florida and El Salto, respectively, have been recognized in the southern part of the Sierra de Fiambalá. The Florida pluton is a leucocratic biotite monzogranite to syenogranite with a porphyritic texture (microcline phenocrysts are 3 × 1.5 cm to 1 × 0.8 cm). The El Salto stock is a leucocratic biotite monzogranite with an equigranular medium-grained (~0.6 cm) texture and shows no sign of deformation. Mineral proportions reveal a dominant monzogranite composition, transitional to granodiorite for the granitic rocks of the Sierra de Fiambalá (Fig. 3).

3.2. The San Blas pluton

The San Blas pluton (SBP) (Báez et al., 2002; Dahlquist et al., 2006) is a semi-ellipsoidal intrusive body of approximately 100 km^2 located in the northwestern part of Sierra de Velasco (Figs. 1 and 2). The host rocks are Carboniferous (343 Ma) porphyritic granitoids of the Asha pluton (Báez et al., 2004) and mylonitic rocks of the TIPA shear zone (Höckenreiner et al., 2003). The contact of the SBP with the surrounding Famatinian granitoids of the TIPA shear zone is sharp and marked by strong topographic relief. Distinctively, the SBP houses several meter-sized mylonitic xenoliths (Alasino, 2002). Moreover, the SBP lacks the penetrative mylonitic deformation of the TIPA shear zone, which is widely found in the porphyritic granitoids of the Sierra de Velasco (regional distribution of mylonites from Aceñolaza et al., 2000; Höckenreiner et al., 2003; Fig. 1).

The dominant rock types in the SBP are porphyritic, biotite monzogranite to syenogranite (Fig. 3) with accessory muscovite. Their petrography is characterized by large microcline crystals (3–15 cm

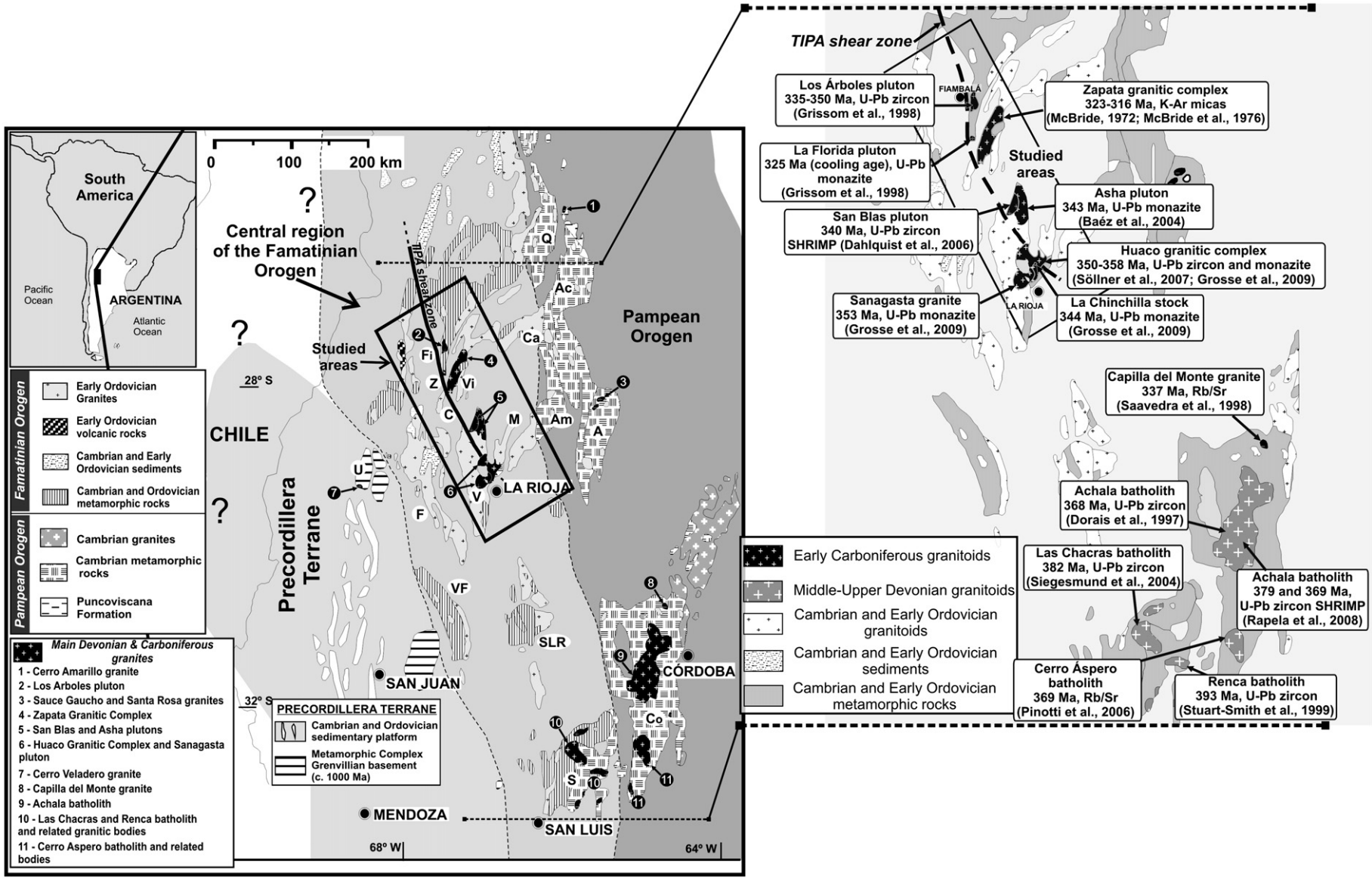

Fig. 1. Geological sketch map of the Sierras Pampeanas, Argentina (after Rapela et al., in press). Main inset shows Middle–Upper Devonian and Early Carboniferous granites in Sierras de San Luis, Córdoba, Velasco, Zapata and Fiambalá. Sierra names: (Q) Quilmes, (Ac) Aconquija, (Fi) Fiambalá, (Z) Zapata, (Vi) Vinquis, (C) Copacabana, (A) Ancasti, (Am) Ambato, (M) Mazán, (V) Velasco, (U) Umango, (F) Famatina, (VF) Valle Fértil, (SLR) Sierras del Sur de La Rioja, (Co) Córdoba, (S) San Luis.

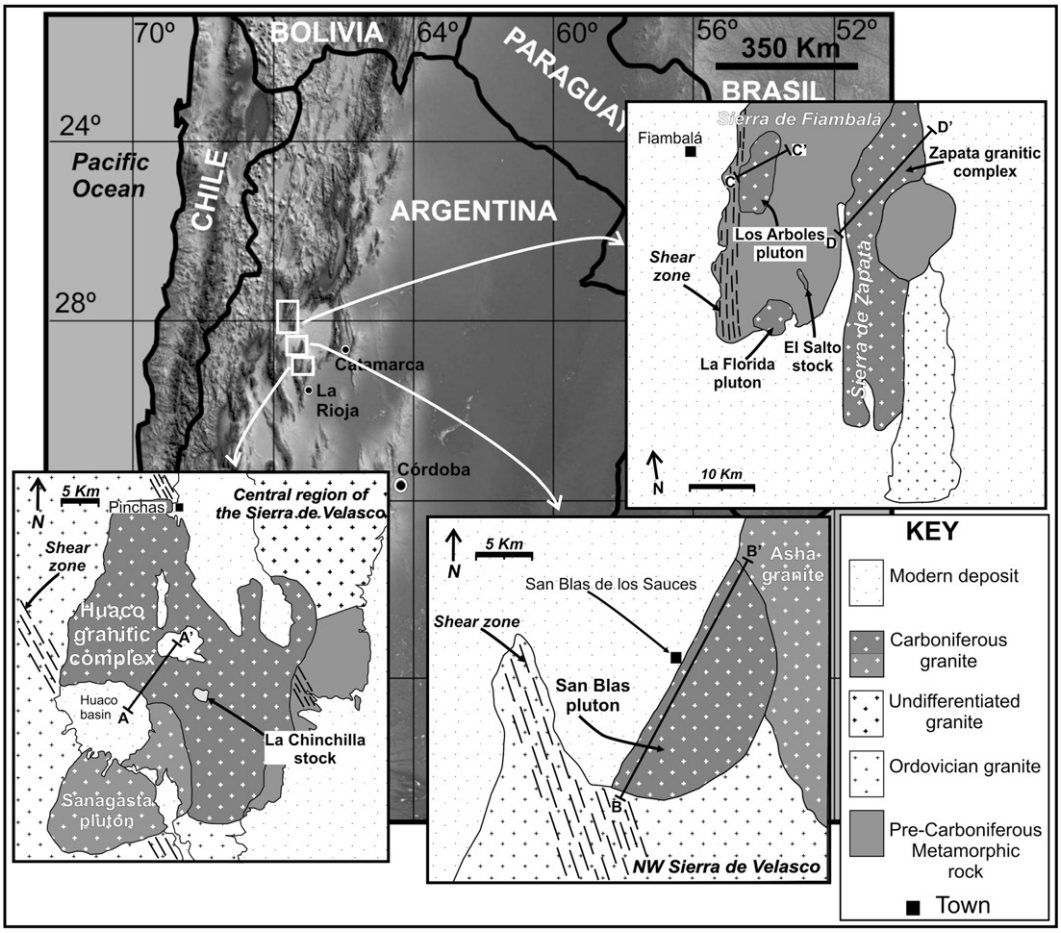

Fig. 2. LANDSAT image showing the Argentina ranges (after Rapela et al., 2007) and schematic geologic map showing the studied granitic rocks. The geologic map of the central region of the Sierra de Velasco is modified from Grosse et al. (2009), the geologic map of the NW region of the Sierra de Velasco is modified from Dahlquist et al. (2006), and the geologic map of the Sierra de Fiambalá is modified from Grissom et al. (1998). The black lines (e.g., A–A′, B–B′, etc.) indicate the approximate locations of the samples included in Table 1, excepting the small granitic bodies such as the La Florida and the El Salto pluton, and the La Chinchilla stock. Abbreviations in all the figures are: SF = Sierra de Fiambalá, SZ = Sierra de Zapata, SV = Sierra de Velasco.

long), which constitute 6–35% of the mode. The matrix is medium-grained, equigranular, and mainly quartz, microcline, and biotite. Miariolitic textures have been observed. Recently, Alba (2008) recognized, according to a modal classification, three additional major facies: (1) feldspar porphyritic felsic granodiorite facies with slight alignment of microcline phenocrysts, localized in the rim of the pluton; (2) the most common and dominant areal K-feldspar porphyritic monzogranite facies, found in the intermediate region of the pluton; and (3) a slightly foliated K-feldspar porphyritic syenogranite facies with a fine-grained matrix, localized in the central area. Felsic and mafic dykes cut the granites. Mafic microgranular enclaves have also been recognized (Báez et al., 2002), mainly in the northern region of the SBP (e.g. Navidad de los Cerros). Recently, a SHRIMP U–Pb zircon age of 340 Ma was reported for the Sam Blas pluton (Dahlquist et al., 2006).

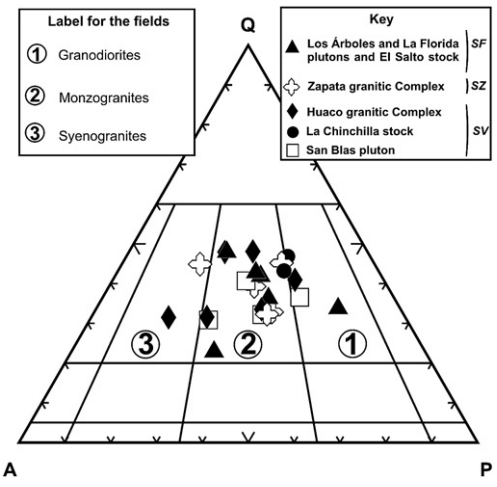

Fig. 3. Modal QAP diagram (Streckeisen, 1976) for the studied granitic rocks. Q = quartz, A = Alkali feldspar, and P = Plagioclase.

3.3. The Zapata granitic complex

The Zapata granitic complex (ZGC) has an areal extent of approximately 470 km^2 (Toselli et al., 1992). Along the studied cross-section (Figs. 1 and 2) metamorphic rocks are very scarce, and they were only observed as small outcrops emergent in the modern sediments. The metamorphic rock is gneiss consisting of plagioclase, quartz, biotite and oxide minerals. The gneiss has an 'S' metamorphic fabric oriented 10°/59°E. Numerous intrusive felsic veins were observed. The relationship between the metamorphic rocks and the ZGC is unknown.

The dominant rock type in the ZGC is biotite monzogranite with zircon, monazite, apatite, oxides, ± amphibole and epidote as accessory minerals. The texture is typically porphyritic with large microcline crystals (5.0 to 3.6 cm long), in a variable grain-sized matrix mainly consisting of quartz, microcline, plagioclase, and biotite. Mineral proportions reveal a dominant monzogranite composition, transitional to syenogranite (Fig. 3).

Two main facies have been recognized: (1) porphyritic monzogranite with large microcline crystals in a coarse-grained matrix and (2) mesocratic porphyritic monzogranite with large microcline crystals in a fine-grained matrix. Both facies are intercalated along the cross-section.

A fabric defined by the alignment of microcline phenocrysts is developed in the ZGC and interpreted as magmatic in origin. The orientation plane of the microcline phenocrysts is variable, although mainly constrained between 260°/54°E and 330°/64°E. The ZGC is intruded by aplitic dykes oriented 5°/76°E.

3.4. The Huaco granitic complex

The Huaco granitic complex (HGC) is an irregular intrusive body with an areal extent of approximately 480 km^2 that outcrops in the central-eastern region of the Sierra de Velasco. The host rocks are Famatinian granitoids, mylonitic rocks of the TIPA shear zone (according to the nomenclature of Höckenreiner et al., 2003) and metamorphic rocks of the La Cébila Formation (Grosse et al., 2009). Different bands of mylonitic rocks are clearly truncated by the HGC. The dominant rock types in the HGC are homogenous porphyritic, biotite monzogranite to syenogranite with secondary muscovite.

Large microcline crystals (5×2 cm and 2×1 cm) occur in a medium-grained matrix consisting of quartz, plagioclase, and biotite. The accessory minerals are apatite, zircon, monazite, and oxide minerals. Mineral proportions reveal a dominant monzogranite composition, transitional to felsic granodiorite and syenogranite (Fig. 3).

A fabric defined by the alignment of microcline phenocrysts is developed in the HGC and is interpreted as magmatic in origin. The orientation of microcline phenocrysts is variable, although the values are mainly constrained between 280° and 320°. The HGC is intruded by aplitic dykes with an orientation of 330°/90°. Semi-ellipsoidal meter-scale felsic equigranular granite enclaves occur within the HGC.

The Chinchilla stock (Grosse et al., 2009) is an undeformed and equigranular (slightly porphyritic towards the center of the stock) monzogranite with distinctive accessory minerals, such as beryl and fluorite, which was emplaced in the HGC. The HGC fabric (defined by the orientation of the microcline phenocrysts) is cut by the Chinchilla stock. The microcline phenocrysts are reoriented at the contact with the Chinchilla stock strongly suggesting an almost synchronous emplacement for both igneous units.

3.5. Sub-volcanic dykes

A common feature recognized in the granitic rocks (LAP, SBP, and HGC) is the presence of relatively mafic sub-volcanic dykes (<60% SiO_2) of dominant moderately alkaline composition (syenodiorite or trachyandesite, Fig. 4 and Table 1). These sub-volcanic dykes are emplaced in the granitic rocks, are dark green or black in colour, and are 1 to 5 m wide. Locally, lobate contacts have been observed between the volcanic phase and the host granitic rocks of the Los Árboles pluton which strongly suggests magma mingling with later disaggregation of the sub-volcanic rocks.

4. Geochronological constraints

U–Pb zircon ages are available for some of the Carboniferous plutons (Fig. 1). Three zircon fractions from the Los Arboles pluton yielded ages between 335 and 350 Ma (Grissom et al., 1998). The San Blas pluton yielded a SHRIMP age of 340±3 Ma (Dahlquist et al., 2006). The Huaco pluton was dated at 354±3.9 Ma (LA-ICP-MS) by Söllner et al. (2007). Grosse et al. (2009) obtained ages of 350±5 Ma and 358±5 Ma (conventional U–Pb dating of monazite) for the same pluton. The Chinchilla stock (which intrudes the Huaco granite) was dated by Grosse et al. (2009) at 344±1.5 Ma (conventional U–Pb monazite dating). For the Zapata granitic complex only K–Ar cooling ages on biotite are available

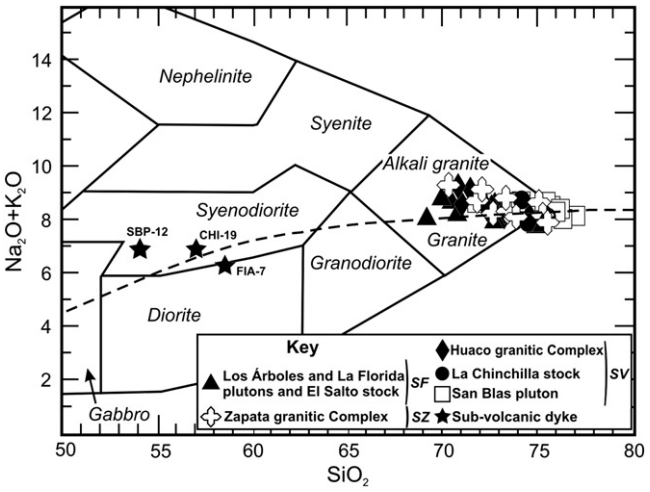

Fig. 4. SiO_2 vs. Na_2O+K_2O variation diagram (after Wilson, 1989). The studied granitic rocks are chemically alkali 'granite' (monzogranite). The alkaline/subalkaline curve is after Miyashiro (1978). Most samples plot in the alkali granite field. The crosses are volcanic rocks in the Los Árboles (FIA-7), San Blas pluton (SBP-12), and Huaco granitic complex (CHI-19).

(323–316 Ma; McBride, 1972; McBride et al., 1976). Other ages of interest for Devonian and Carboniferous plutons in the Sierras Pampeanas are summarized in Fig. 1. Carboniferous plutonism took thus place between 335 and 360 Ma (Fig. 1), i.e., in the Mississippian, and cooled to mica blocking temperatures at ca. 315 Ma (Söllner et al., 2007). These ages match well with those cooling ages obtained from biotite in the meta-granitic rocks near the TIPA shear zone in the Sierra de Copacabana (mean age 300±4 Ma, Höckenreiner et al., 2003). These data strongly suggest an extended Carboniferous heating process affecting the whole crust.

5. Rock geochemistry

Major- and trace element compositions for 46 representative samples from the San Blas and Los Árboles plutons, the Zapata and Huaco granitic complexes, the small granitic bodies (La Florida pluton and the El Salto and the La Chinchilla stock), and the sub-volcanic dykes are presented in Table 1. The analytical methods are described in electronic Appendix A. The black lines in Fig. 2 (e.g., A–A′, B–B′, etc.) indicate the approximate location of the samples included in Table 1, except the small granitic bodies such as the La Florida pluton and the El Salto and the La Chinchilla stocks.

5.1. Major element

The data show that these rocks are felsic or evolved in composition, and their SiO_2 content varies within a restricted range from 69.2 to 76.4 wt.% (representative data in Table 1 and all data are found in a supplemental electronic data table). On the alkalis vs. silica classification diagram of Wilson (1989), the rocks plot dominantly at the silica-rich end of the field of alkaline granitoids (Fig. 4). The sub-volcanic dykes emplaced in the granites have a moderate alkaline composition (Fig. 4).

The granitic rocks are metaluminous to slightly peraluminous (aluminium saturation index, ASI = 0.98–1.15, Fig. 5) and have a relatively high agpaitic index (0.64–0.90, average = 0.75, Table 1). The monzogranites are poor in CaO (0.51–1.29 wt.%) and extremely rich in FeO^t relative to MgO with high $FeO^t/(FeO^t+MgO)$ ratios (0.88–0.98). They are also enriched in TiO_2 relative to MgO (mostly $TiO_2/MgO>1$) and are moderately enriched in total alkalis (7.81–9.30 wt.%), with relatively high K_2O content ($K_2O/Na_2O = 0.85–2.03$ wt.%). The granitic rocks generally follow the alkali-calcic and ferroan trend on the Na_2O+K_2O-CaO and $FeO^t/(FeO^t+MgO)$ vs. SiO_2 diagrams of Frost et al. (2001) (Fig. 6).

Table 1
Representative major and trace element whole-rock data for the granitic complexes.

	Los Árboles pluton			LFP	SVD	Zapata Granitic Complex					Huaco Granitic Complex		
	Western Zone		Eastern Zone										
Facies	PG	PG	EG	PG		Ap	PG	*FMPG*	*PG*	*FMPG*	PG	FMPG	PG
Locality	27°44′29″ 67°32′31″	27°44′17″ 67°31′26″	27°44′34″ 67°30′04″	27°58′50″ 67°32′58″	27°44′32″ 67°32′36″	27°53′56″ 67°22′22″	27°53′39″ 67°22′20″	27°53′27″ 67°21′27″	27°53′17″ 67°21′15″	27°27′55″ 67°16′34″	29°09′48″ 67°00′22″	29°10′02″ 67°00′36″	29°11′23″ 67°01′45″
Sample	FIA-03	FIA-22	FIA-17	FIA-24	FIA-7	ZAP-27	ZAP-29	ZAP-32	ZAP-33	ZAP-36	HUA-01	HUA-07	HUA-12
wt.%													
SiO_2	69.21	72.77	74.5	74.96	58.57	75.11	73.46	75.57	71.86	73.34	71.05	72.62	73.3
TiO_2	0.40	0.37	0.07	0.14	1.61	0.06	0.13	0.14	0.25	0.12	0.23	0.19	0.19
Al_2O_3	12.41	12.13	11.98	12.03	13.41	12.31	12.32	11.66	13.1	12.18	13.98	12.93	13.39
Fe_2O_3	3.69	3.33	1.45	1.86	7.56	1.31	1.93	2.01	2.41	2.04	2.3	2.03	2.27
MnO	0.05	0.05	0.02	0.03	0.11	0.05	0.04	0.03	0.04	0.03	0.04	0.03	0.05
MgO	0.46	0.31	0.03	0.11	2.75	0.05	0.1	0.09	0.19	0.07	0.27	0.22	0.15
CaO	1.24	1.23	0.64	0.77	3.97	0.69	0.85	0.82	1.06	0.88	1.04	0.6	0.84
Na_2O	3.00	2.86	3.29	2.99	3.08	3.27	3.18	2.91	3.06	3.29	3.12	2.81	3.18
K_2O	5.07	5.09	4.92	4.82	3.22	5.43	5.18	5.03	5.7	4.98	5.51	5.7	5.19
P_2O_5	0.14	0.11	0.02	0.05	0.41	0.02	0.04	0.03	0.07	0.02	0.2	0.13	0.14
LOI	2.83	1.89	1.66	1.76	4.31	1.92	1.66	1.66	1.73	1.84	1.54	1.59	1.63
Total	98.5	100.14	98.58	99.52	99.00	100.23	98.89	99.95	99.47	98.79	99.28	98.85	100.33
(ppm)													
Be	4	6	6	8	6	7	8	7	7	7	12	7	8
Sc	5	5	2	5	14	5	3	4	5	4	4	3	4
V	18	14	<5	<5	136	8	6	6	8	<5	9	11	<5
Cr	170	70	140	110	50	100	160	160	50	60	80	120	170
Co	5	3	<1	1	18	2	1	1	2	<1	2	2	1
Cu	140	10	<10	<10	20	30	10	10	<10	<10	<10	20	20
Zn	60	50	<30	<30	90	50	40	30	40	30	60	60	60
Cs	3.8	4.7	10.1	9.2	6.8	14.4	12.3	14	11.5	12	24.9	13.5	31.7
Rb	235	300	650	467	292	429	511	470	372	556	408	420	450
Sr	91	81	9	18	213	20	32	27	74	25	73	49	60
Ba	326	286	31	64	333	55	116	81	335	88	267	184	251
La	93.4	87	53.2	57.6	62.7	111	59.6	89	53.4	99.8	41.5	41.9	51.6
Ce	195	180	121	137	137	251	143	198	118	231	96.7	102	120
Pr	20	18.6	13.7	15.2	15.1	27.3	16.8	21.4	13.2	25.9	11.3	11.8	13.4
Nd	67.1	61.7	51.5	55.7	53.9	92.3	64.5	71.5	46.3	89.1	41.6	43.6	49.1
Sm	12.1	11.2	12.1	12.4	11.3	17.1	15.1	14.3	9.71	19.5	8.62	9.75	10.5
Eu	1.13	1.08	0.18	0.32	1.7	0.82	0.5	0.42	1.01	0.48	1.05	0.66	1.19
Gd	9.76	9.21	12.4	12.2	10.1	13.6	13.9	11.3	8.65	16.2	7.21	8.17	8.05
Tb	1.73	1.66	2.86	2.75	1.9	2.34	2.77	2.13	1.79	3.24	1.4	1.59	1.62
Dy	9.7	9.5	19.1	17.9	11.2	12.5	17.0	12.5	10.6	20	7.14	9.14	9.59
Ho	1.82	1.83	3.93	3.57	2.18	2.31	3.33	2.39	1.99	3.86	1.16	1.53	1.74
Er	5.29	5.41	12.7	11.0	6.56	6.54	10.5	7.36	5.85	11.7	3.00	4.12	5.19
Tm	0.78	0.81	2.05	1.72	1.02	0.94	1.75	1.12	0.91	1.86	0.4	0.57	0.82
Yb	4.73	5.14	13.1	10.7	6.46	5.55	11.2	7.32	5.72	11.6	2.25	3.32	5.23
Lu	0.68	0.74	1.83	1.49	0.91	0.78	1.62	1.04	0.84	1.63	0.3	0.45	0.74
U	7.46	8.8	20.7	10.1	9.98	6.95	12.1	11.9	7.17	12.8	7.83	6.93	6.2
Th	42.8	50.1	77.1	39.9	33.6	57.8	53	70.1	28.4	78.6	27.3	28.1	30.1
Y	54.2	56.9	130	113	69.3	68	125	81.2	57.9	118	35.5	53.3	54.2
Nb	25.2	27	68.3	42.2	51.3	34.8	39.3	40.6	34.9	61.7	25.2	20.2	33.1
Zr	337	303	168	157	255	264	183	192	248	188	195	124	191
Hf	9.2	8.4	7.4	5.6	7.1	8.3	6.3	6.9	6.9	7.4	5.1	3.7	5.6
Ta	2.37	2.78	7.86	6.19	5.04	2.94	5.92	5.49	4.3	9.02	3.27	2.05	4.93
Pb	30	24	34	27	17	34	41	35	32	37	35	33	30
Ga	22	23	26	21	22	25	25	22	21	24	21	22	24
Mo	18	9	14	12	16	11	18	16	6	8	8	12	16
Sn	8	10	4	3	7	6	12	12	9	8	11	7	16
W	9.5	4.7	6.5	11.5	3.1	3.1	3.0	7.8	1.7	7.7	3.3	5.6	4.7
Eu/Eu*	0.32	0.33	0.05	0.08	0.49	0.17	0.11	0.1	0.34	0.08	0.41	0.23	0.4
M	1.50	1.38	1.46	1.33	2.01	1.38	1.42	1.38	1.45	1.43	1.36	1.31	1.32
T_{zr}(°C)	847	839	792	790		833	797	803	821	798	806	771	807

Major element oxides and trace elements were analysed by ACTLABS Canada (analytical details are found in electronic Appendix A). Total iron as Fe_2O_3; major element oxides in wt. %, trace elements in ppm. Abbreviations: PG: Porphyritic granite; EG: Equigranular granite; LFP: La Florida pluton; SVD: Sub-volcanic dyke; FMPG = Fine matrix porphyritic granite; Ap: Aplite; CMPG: Coarse-grained matrix porphyritic granite. LFB = Lachlan Fold Belt (Australia), KR = Kokshaal Range (Kyrgyzstan). *n* = average samples, nr = not reported. $T_{Zr} = 12{,}900/[2.95 + 0.85\,M + \ln(496{,}000/Zr_{melt})]$, where $D^{Zr,zircon/melt} = (496{,}000/Zr_{melt})$, is the ratio of Zr concentrations (ppm) in zircon to that in the saturated melt; M is a compositional factor that accounts for dependence of zircon solubility on SiO_2 and peraluminosity of the melt [$(Na + K + 2 \cdot Ca)/Al \cdot Si$), all in cation fraction]. The geothermometer is calibrated for $M = 0.9$ to 1.7. Equation and Zr concentrations (ppm) in zircon (= 496,000 ppm) from Miller et al. (2003).

[a] The LFB average was taken from Chappell and White (1992).

[b] The KR average was calculated using the data shown in Table 1 from Konopelko et al. (2007), using samples of the Uch-Koshkon felsic granite.

5.2. Trace element

The concentration ranges for the High Field Strength Elements (HSFE), such as Y, Nb, Ga, Ta, U, Th etc., are comparable to those reported in anorogenic granitic complexes such as the A-type granites of the Lachlan Fold Belt in Australia (data in Table 1 from Chappell and White, 1992) or the Hercynian A-type granites of the Kokshaal range in Kyrgyzstan (data in Table 1 from Konopelko et al., 2007). The

			San Blas Pluton						La Chinchilla stock		LFB[a]	KR[b]
PG	AP	SVD	PG	CMPG	FMPG	PG	AP	SVD	EG	EG		
29°11′48″ 67°59′06″	29°08′02″ 67°00′11″	29°08′02″ 66°58′07″	28°32′31″ 67°09′11″	28°27′21″ 67°05′55″	28°27′14″ 67°06′01″	28°29′11″ 67°04′55″	28°27′20″ 67°05′56″	28°27′56″ 67°05′36″	29°10′40″ 66°58′21″	29°10′21″ 66°58′20″	*Av. n =43*	*Av. n =5*
HUA-13	HUA-5	CHI-19	SBP-15	SBP-07	SBP-09	SPB-10	SBP-08	SBP-12	CHI-15	CHI-18		
72.39	73.28	57.07	73.92	76.37	71.83	76.01	76.24	54.11	74.54	75.33	73.83	73.72
0.19	0.06	1.75	0.23	0.13	0.38	0.11	0.02	1.9	0.05	0.05	0.28	0.16
13.11	13.45	15.26	12.84	11.85	13.57	11.99	13.22	15.02	12.26	12.79	12.79	13.45
2.02	1.31	8.72	2.39	1.79	3.09	1.8	1.03	10.09	1.52	1.49	0.84	0
0.03	0.07	0.14	0.04	0.03	0.05	0.03	0.05	0.16	nd	nd	1.54	1.76
0.16	0.07	3.57	0.17	0.07	0.33	0.03	0.00	3.94	0.06	0.06	0.05	0.04
0.97	0.31	4.81	0.8	0.68	1.15	0.66	0.46	5.13	0.08	0.05	0.29	0.16
2.79	3.42	3.93	3.2	2.91	3.29	3.05	4.35	3.76	0.62	0.65	1.04	1.01
5.66	4.75	3.05	5.5	5.16	5.39	5.29	4.1	3.21	3.74	3.8	3.42	3.27
0.11	0.13	0.74	0.11	0.05	0.21	0.04	0.02	0.86	4.2	4.47	4.67	5
1.65	1.81	1.49	0.55	0.69	0.7	0.64	0.49	1.66	0.02	0.02	0.07	0.05
99.08	98.65	100.53	99.75	99.73	99.99	99.64	99.98	99.84	1.81	1.8	nr	0.92
									98.9	100.51	98.82	99.53
6	8	6	8	11	16	9	23	7	7	21		
4	3	13	5	5	5	3	1	16	3	3		
5	8	116	7	8	13	6	20	119	6	43		
110	100	100	40	<20	<20	30	30	50	150	170		
1	<1	23	1	<1	2	<1	<1	21	1	<1		
10	<10	20	<10	20	<10	20	<10	20	70	20		
40	40	80	50	50	40	30	<30	90	40	30		
26.3	34	77.4	15.3	38.8	31.1	20.5	140	36.6	23.8	22		
382	559	192	453	482	470	568	1000	255	684	687		
64	19	490	45	31	63	16	4	419	8	9		
233	105	244	108	79	155	45	10	314	16	25		
49.3	11	32.9	75.3	64.2	52.1	72	13	45.5	15.2	17.8		
112	25.9	72.6	165	142	117	170	38.1	102	41.9	49.7	130	100
12.5	2.92	8.34	18.1	15.9	13.6	20	5.3	12.3	5.63	6.47		
44.8	11.9	33.4	59.5	53.5	47.5	73.9	26.0	48.0	29.5	31.3		
9.24	2.67	6.96	11.1	10.4	9.58	16.8	7.95	9.87	8.55	9.55		
1.23	0.27	2.09	0.65	0.5	0.9	0.43	0.06	2.3	0.17	0.19		
7.01	2.55	5.75	8.86	8.55	8.21	15.3	8.42	8.89	9.23	10.6		
1.26	0.68	0.97	1.48	1.48	1.39	3.03	1.99	1.43	2.27	2.67		
6.92	4.76	5.37	8.19	8.43	8.04	19	13.9	7.95	16	18.3		
1.2	0.96	0.93	1.5	1.57	1.46	3.72	2.91	1.48	3.24	3.73		
3.48	3.03	2.52	4.32	4.58	4.22	11.4	9.99	4.26	10.6	11.6		
0.55	0.59	0.35	0.62	0.70	0.66	1.88	2.01	0.65	1.84	2.04		
3.62	4.22	2.17	3.7	4.22	4.2	11.6	14.1	3.98	12.4	13.2		
0.52	0.61	0.32	0.5	0.6	0.59	1.59	2.07	0.54	1.82	1.88		
5.93	9.06	7.58	12.1	8.83	6.04	10.3	28.3	6.09	33.3	34.4	5	10
28.2	9.17	5.76	73.4	82.7	46.1	86.3	31.9	17.5	35.9	43.3	24	51
36.5	32.1	27.4	45.1	45.1	45.8	113	103	44.2	125	142	71	65
23	33.1	33.9	33.6	33.3	37.3	81.1	45.7	46.5	54.5	58.2	26	26
156	36	238	234	161	261	208	81	247	104	104	322	185
4.6	1.7	5.4	7.1	5.9	7.5	9.2	6.4	6.5	5.7	5.7		
2.84	5.87	4.18	3.15	4.94	6.08	6.59	22.8	4.04	13.8	15.0		
29	28	10	29	25	17	29	28	10	36	33		
22	26	21	24	21	23	30	34	21	29	29	22	24
14	9	5	<2	<2	<2	2	<2	3	14	16		
7	22	10	9	8	12	6	16	6	41	41		
4.1	16.3	5.7	2.4	10.5	12.1	5.4	7.8	2.8	6.4	5.0		
0.47	0.32	1.02	0.2	0.16	0.31	0.08	0.02	0.75	0.06	0.06		
1.36	1.19	2.25	1.41	1.35	1.45	1.38	1.32	2.44	1.34	1.34		
787	683		819	790	827	811	735		754	754		

granitoids also plot in the field of A-type granites on the discrimination diagrams of Whalen et al. (1987) (Fig. 7). Primitive mantle-normalized spider diagrams show marked negative Ba, Nb, Sr, P (with the exception of the Huaco granitic complex which only shows a moderate negative anomaly), Eu and Ti anomalies and significant enrichment in Rb, Th, U, and Pb (Fig. 8). Rare earth element (REE) abundances vary from 116 to 554 ppm. The REE patterns are flat or slightly light REE enriched (LREE) with significant negative Eu

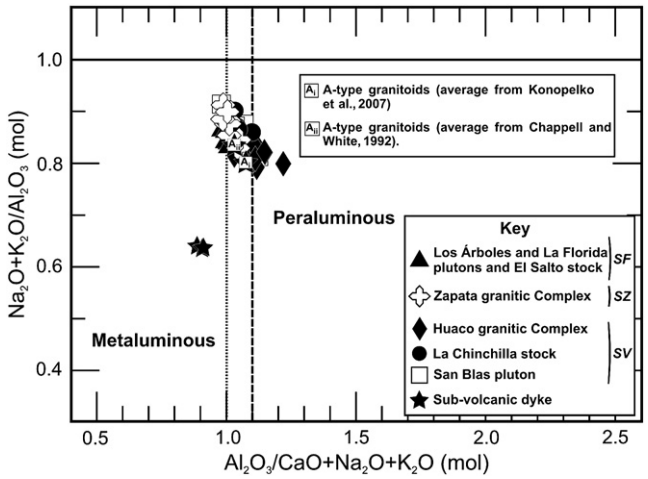

Fig. 5. Alumina saturation index (ASI) in the studied granitic rocks. Most of the samples are constrained to ASI = 1.0–1.1, with high values for the agpaitic index. ASI=1 from Shand (1927), ASI=1.1 from Chappell and White (1992).

anomalies (Fig. 8) These patterns are similar to those reported for A-type granites (e.g., Scheepers, 2000; Konopelko et al., 2007).

6. Biotite chemistry

The studies of Abdel Rahman (1994) demonstrate that the compositions of igneous biotites reflect the nature of their parental host magmas. Biotites crystallized from Early- to Mid-Ordovician calc-alkaline granitic magmas (Famatinian Orogen) are significantly different from those biotites crystallized from the Early Carboniferous granitic magmas (representative data in Table 2 and all data are found in a supplemental electronic data table, analytical methods are described in electronic Appendix A).

Biotites from the calc-alkaline suite of the Famatinian Orogen are moderately enriched in MgO with $FeO^t/MgO = 1.72–1.76$ and occupy a narrow field in Fig. 9a. Biotites from Ordovician peraluminous rocks, such as the Tuaní Granite unit, plot below the general trend of the Ordovician metaluminous calc-alkaline biotites and have $FeO^t/MgO = 1.64$. Biotites crystallized from the A-type plutons have very high FeO relative to MgO, with $FeO^t/MgO = 8.46–59.52$ and mostly plot in the field of anorogenic alkaline granites (Fig. 9a).

Fluorine data is not available for the whole-rock samples. However the distinctive high-F biotites (together with very high $[Fe^{2+}/(Fe^{2+} + Mg)]$ ratios>0.8, representative data in Table 2 and all data can be found in a supplemental electronic data table and Fig. 9b) strongly suggest that the magmas had relatively high HF/H_2O ratios. The more complete data for the San Blas pluton indicate a progressive F-enrichment with magmatic differentiation (Fig. 9b). Similarly the biotites from the more evolved granitic facies of the Los Árboles pluton (biotite leucocratic facies) contain the highest values of F (representative data in Table 2 and all data can be found in a supplemental electronic data table and Fig. 9b). The biotites from the Huaco and Zapata granitic complex rocks also have relatively high values of F (Fig. 9b). The F-rich character of the magma is further confirmed by the presence of REE-rich fluorcarbonates in the San Blas pluton (unpublished data) and fluorite (up to 1% modal) in the La Chinchilla stock (Grosse et al., 2009).

Muñoz (1984, 1992) and Icenhower and London (1997) have presented models for calculating the F and Cl contents of aqueous and melt phases co-existing with biotite. Here we are interested in the F and Cl content of the magma. Representative calculated F and Cl

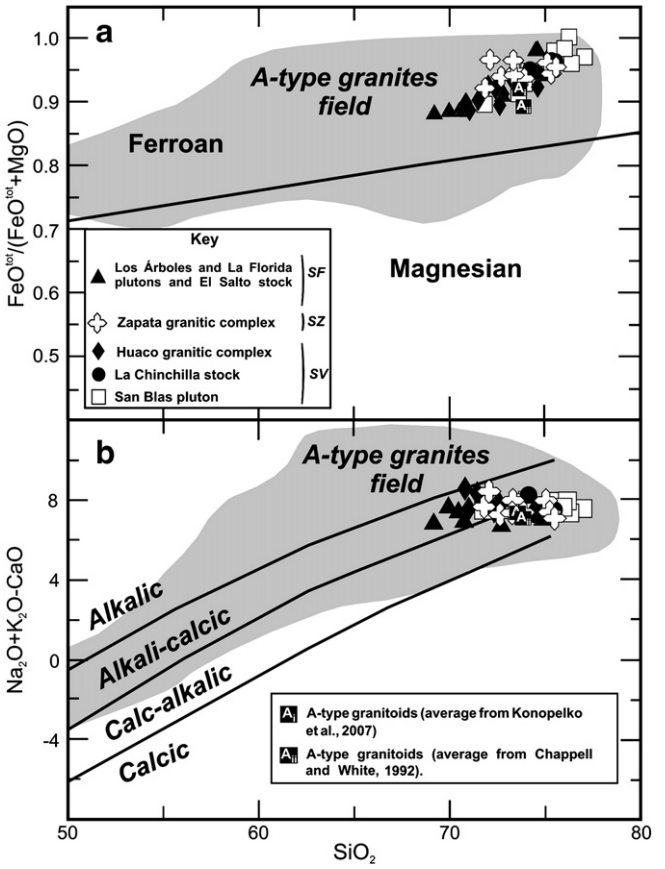

Fig. 6. Studied granites plotted on the classification diagrams of Frost et al. (2001): (a) $Na_2O + K_2O - CaO$ vs. SiO_2, wt.% and (b) $FeO^t/(FeO^t + MgO)$ vs. SiO_2, wt.% (b). The A-type granite field is after Frost et al. (2001). A granitic Famatinian calc-alkaline suite is also plotted in this diagram (See text for discussion). Abbreviation: SCh = Sierra de Cheepes. Di–Tn = diorites and tonalites, G = granodiorites, PG = porphyritic granodiorites, Mz = monzogranites (data from Dahlquist et al., 2005b).

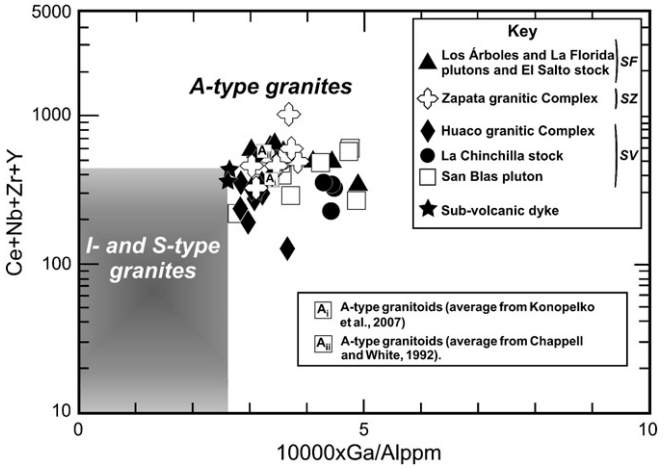

Fig. 7. Ce + Nb + Zr + Y vs. 10,000 × Ga/Al granite discrimination diagram (Whalen et al., 1987).

concentrations for magma at 800 °C (using the equations of Muñoz, 1992) are reported in Table 2 (all data can be found in a supplemental electronic data Table) and shown graphically on Fig. 9c. We did the same calculations using the model of Icenhower and London (1997). For this model the calculated Cl melt concentrations are essentially

Fig. 8. Primitive mantle-normalized (Sun and McDonough, 1989) spider diagrams and chondrite-normalized (Nakamura, 1974; Boynton, 1984) REE plots. The granitic bodies have similar compositions to those reported for other A-type granites (e.g., Scheepers, 2000; Konopelko et al., 2007). Sub-volcanic dikes: (a) FIA-7, (b) CHI-19, (c) SBP-12.

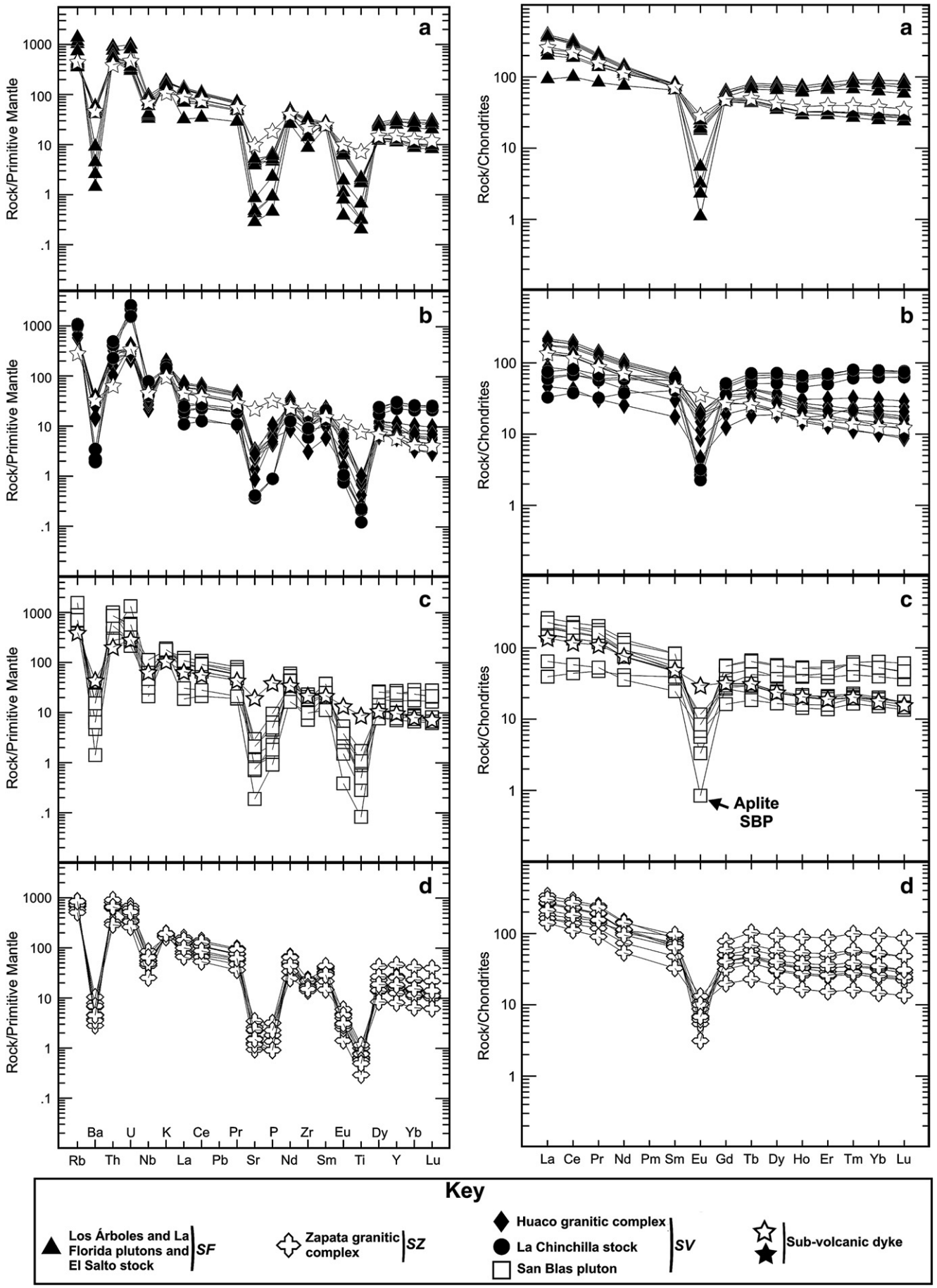

Table 2
Representative compositions of biotites from the Ordovician (Famatinian Orogen) calc-alkaline I- and S-type granitic rocks of the Sierras Pampeanas, Argentina and for biotites in the Carboniferous granites.

Rock type	I-type	I-type	S-type
Sample	ASP-120	ASP-120/1	32-JEOL-00
Lithology	Hbl-Bt Gde	Hbl-Bt Gde	Crd- Qtz-rich Gtoid
wt.%			
SiO_2	35.53	35.68	35.59
TiO_2	2.83	2.78	2.49
Al_2O_3	16.38	16.31	19.99
FeO	18.68	19.2	17.12
MnO	0.35	0.32	0.58
MgO	10.52	10.2	9.8
CaO	0.03	0.02	0.02
Na_2O	0.14	0.09	0.22
K_2O	9.7	10.05	9.52
F	0.16	0.01	0.23
Cl	0.04	0.05	0.04
Total	94.36	94.71	95.65
O_F_Cl	0.08	0.02	0.11
CTotal	94.28	94.69	95.54
FeO^t/MgO	1.78	1.88	1.75
T(°C)	800	800	800
F_{melt} (ppm)	12	166	468
Cl_{melt} (ppm)	156	95	0

Sample	FIA17/2	FIA17/5	FIA17/6	ZAP33/46	ZAP33/49	ZAP33/51
wt.%						
SiO_2	36.02	36.18	35.45	34.41	34.35	34.40
TiO_2	2.09	1.57	1.47	3.09	2.95	3.11
Al_2O_3	18.90	19.63	20.32	15.01	15.87	14.94
FeO	27.55	27.83	27.36	29.24	27.75	28.54
MnO	0.35	0.38	0.32	0.49	0.35	0.44
MgO	0.72	0.71	0.65	3.34	3.21	3.68
CaO	0.00	0.06	0.03	0.01	0.00	0.00
Na_2O	0.13	0.13	0.13	0.08	0.06	0.06
K_2O	9.46	9.33	9.34	9.37	9.42	9.38
F	1.15	1.29	1.05	0.25	0.24	0.47
Cl	0.39	0.40	0.40	0.25	0.21	0.28
Total	96.81	97.52	96.52	95.56	94.40	95.29
O_F_Cl	0.57	0.63	0.53	0.16	0.15	0.26
CTotal	96.24	96.89	95.99	95.40	94.25	95.03
FeO^t/MgO	38.26	39.20	42.09	8.75	8.64	7.76
T (°C)	800	800	800	800	800	800
F_{melt} (ppm)	4430	3860	2860	590	910	1180
Cl_{melt} (ppm)	1050	960	120	520	630	730

Sample	HUA12/10	HUA12/9	SBP2/1	SBP2/3	SBP3/3	TUY12/2	TUY12/3
wt.%							
SiO_2	34.47	36.13	34.66	33.85	35.03	34.90	34.03
TiO_2	2.10	2.40	2.08	2.53	2.10	3.08	2.93
Al_2O_3	19.03	18.93	18.26	18.21	18.97	18.79	18.99
FeO	26.35	25.31	29.39	30.12	27.69	27.16	26.88
MnO	0.57	0.71	0.61	0.52	0.65	0.52	0.39
MgO	2.28	2.57	0.63	0.49	0.77	2.56	2.55
CaO	0.00	0.01	0.09	0.15	0.07	0.00	0.09
Na_2O	0.08	0.10	0.09	0.12	0.13	0.12	0.10
K_2O	9.58	9.75	9.02	9.16	9.16	9.77	9.04
F	0.60	1.07	1.43	0.98	1.25	0.49	0.14
Cl	0.07	0.02	0.25	0.31	0.30	0.10	0.15
Total	95.12	97.00	96.51	96.44	96.12	97.49	95.29
O_F_Cl	0.27	0.46	0.66	0.48	0.59	0.23	0.09
CTotal	94.85	96.54	95.85	95.96	95.53	97.26	95.2
FeO^t/MgO	11.56	9.85	46.65	61.47	35.96	10.61	10.54
T (°C)	800	800	800	800	800	800	800
F_{melt} (ppm)	5610	1880	4440	4750	4860	360	350
Cl_{melt} (ppm)	650	90	830	840	740	800	260

Total iron measured as FeO. Abbreviations: Gde: Granodiorite, Gtoid: Granitoid. Mineral abbreviations from Kretz (1983). Data from Dahlquist et al. (2005a,b) and Alasino (2007). Calculated F and Cl following Muñoz (1984, 1992). Structural formulae for biotites and calculated F_{melt} and Cl_{melt} are found in the supplemental electronic Table.

identical to those of the Muñoz (1992) model, but for F there is a significant divergence in the calculated values which increase with decreasing mg# (increasing Fe content of the biotite). For example, for sample SBP-2/1 the Muñoz (1992) model gives a calculated F value of 5800 ppm while the Icenhower and London (1997) model gives a calculated F value of 42,200 ppm. It should be noted that the Icenhower and London (1997) model was not calibrated for low mg# (high Fe) biotites and values derived from this model for very

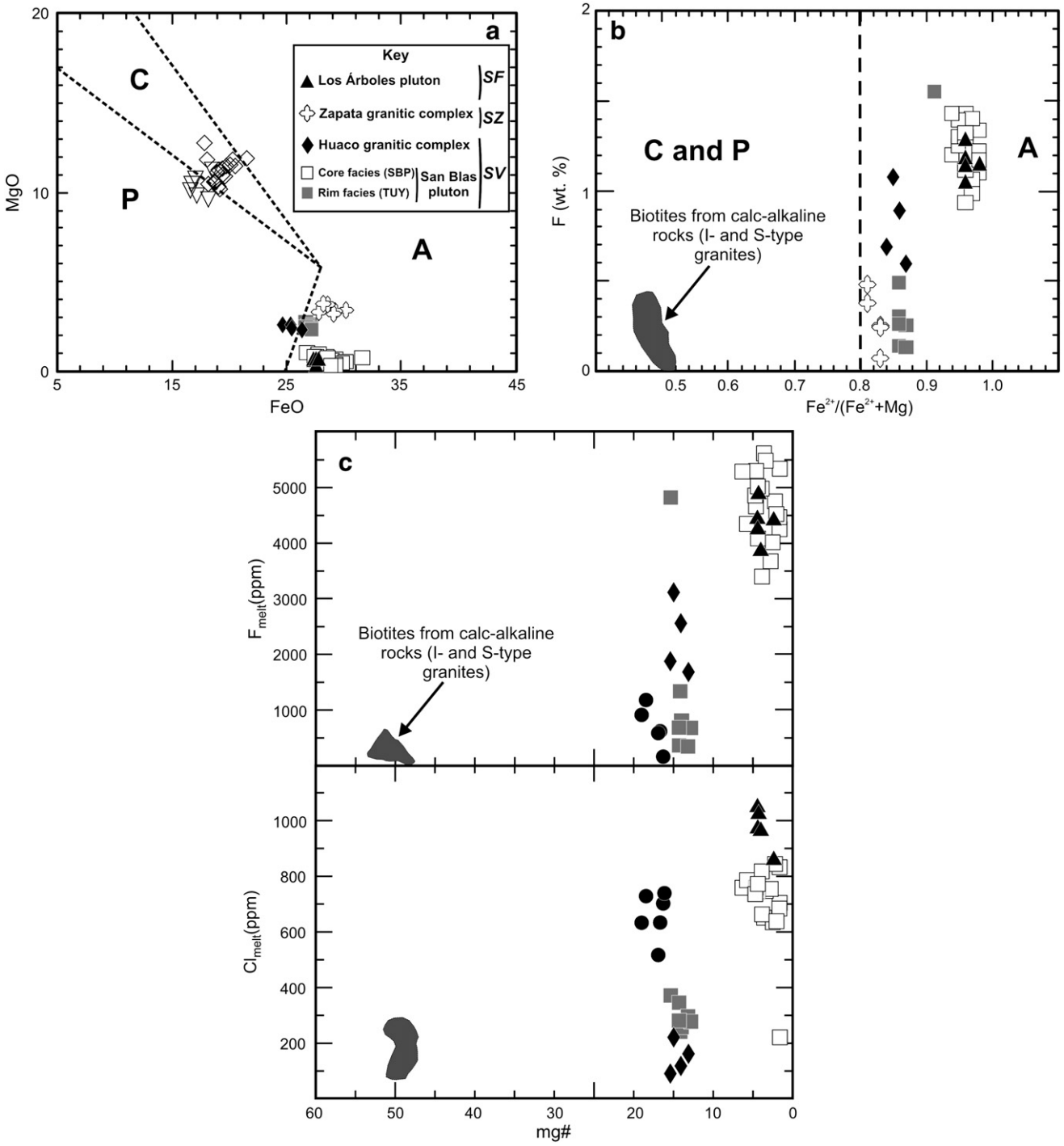

Fig. 9. Mineral chemistry for biotites crystallized from calc-alkaline metaluminous and peraluminous granites of Early Ordovician age and biotites crystallized from the studied granites. (a) FeO vs. MgO biotite discriminant diagram after Abdel Rahman (1994): biotite in anorogenic alkalines suites (A field), biotite in peraluminous granites (S-type granites, empty triangles) (P field), and biotite in metaluminous calc-alkaline granites suite (I-type granites, empty diamonds) (C field). (b) F vs. $Fe^{2+}/(Fe^{2+}+Mg)$ diagram for biotites. Biotite in anorogenic alkaline suites (A field) have $Fe^{2+}/(Fe^{2+}+Mg)>0.8$ and higher F content. (c) Plot of mg# vs. calculated F and Cl using the equations of Muñoz (1984, 1992). The calculated magma F and Cl content (together with the mg #) for these A-type granitoids (F = 580–5600 ppm and Cl = 90–1180 ppm, see Section 6) is generally higher than that for calc-alkaline granites (F = 0–470 ppm and Cl = 0–250 ppm). SBP: core samples and TUY: rim samples from the San Blas pluton (data in Table 2 and supplemental electronic data table).

iron-rich biotites range up to 10 wt.% F in the melt, an unrealistically high-F content. The calculated F values reported here are based on the Muñoz (1992) model.

A component of the definition of A-type granites is that the melt contains relatively high F, but this is rarely quantified. In this paper we present one of the first attempts to provide quantitative data on magma F (and Cl) content. Biotites in the Early Ordovician granitic rocks with calc-alkaline signature (formed during the Famatinian orogen, NW Argentina, Dahlquist et al., 2005a, 2008) have mg# ~50 and the magmas are characterized by both low F (0 to 470 ppm) and Cl (0 to 250 ppm). For the A-type granitoids, biotite mg#s vary from 19 to 2, and for each pluton or complex there is a restricted range in the mg# of the biotites and the magma F and Cl content (Table 2 and supplemental electronic data table, and Fig. 9c). The Los Árboles (F = 3850 to 4900 ppm, Cl = 860 to 1050 ppm) and San Blas (F = 3400 to 5600 ppm, Cl = 640 to 850 ppm) plutons have the

Table 3a
Rb–Sr composition of representative samples from the studied granitic rocks.

Samples	SiO_2 (wt.%)	Rb	Sr	$^{86}Rb/^{87}Sr$	$(^{87}Sr/^{86}Sr)_{today}$	$(^{87}Sr/^{86}Sr)t$
t = 323 Ma						
ZAP-26	72.70	438.1	53.1	24.1347	0.820759	0.709805
ZAP-27	75.11	506.8	19.3	78.4302	1.038146	0.677580
ZAP-33	71.86	378.9	73.1	15.1039	0.780833	0.711396
ZAP-35	73.37	313.7	44.1	20.7779	0.805605	0.710083
t = 354 Ma						
HUA-4	74.61	380.6	64.2	17.2930	0.791567	0.704417
HUA-6	72.79	390.6	57.0	20.0153	0.805095	0.704225
HUA-13	72.39	392.8	30.5	37.8985	0.882489	0.691495
HUA-14	70.86	365.0	66.4	16.0275	0.786958	0.706185

The decay constants used in the calculations are $\lambda^{87}Rb = 1.42 \times 10^{-11}$ and $\lambda^{147}Sm = 6.54 \times 10^{-12}$ year^{-1} recommended by the IUGS Sub-commission for Geochronology (Steiger and Jäger, 1977). Epsilon-Sr (εSr) values were calculated relative to a uniform reservoir present day: $(^{86}Rb/^{87}Sr)_{UR}^{today} = 0.0827$; $(^{87}Sr/^{86}Sr)_{UR}^{today} = 0.7045$. Epsilon Nd ($\varepsilon_{Nd}$) values were calculated relative to a chondrite present day: $(^{143}Nd/^{144}Nd)_{CHUR}^{today} = 0.512638$; $(^{143}Sm/^{144}Nd)_{CHUR}^{today} = 0.1967$.
t = time used for the calculation of the isotopic initial ratios. T_{DM}^{*} = calculated according to De Paolo et al. (1991).
The ages are: FIA-17 (335 Ma, Grissom et al., 1998), HUA-4 (354 Ma, Söllner et al., 2007), SBP-15 (340 Ma, Dahlquist et al., 2006), ZAP (323 Ma, McBride, 1972; McBride et al., 1976).

highest calculated magma F and Cl contents. The Huaco granitic complex (F = 1700 to 3100 ppm, Cl = 90 to 220 ppm) has higher calculated magma F content and lower calculated magma Cl content than the Zapata granitic complex (F = 580 to 1180 ppm, Cl = 510 to 740 ppm). It should be noted that while the calculated magma F and Cl content for these A-type granitoids is generally higher than that for calc-alkaline granites, the values are not excessively high, i.e., water is still a significant part of the volatile component of the magmas.

7. Sr and Nd isotope systematics

7.1. Rb–Sr isotopes

Initial $^{87}Sr/^{86}Sr$ ratios of ca. 0.7088 (for a U–Pb SHRIMP zircon crystallization age of 340 ± 3 Ma) were reported by Dahlquist et al. (2006) for the San Blas pluton. This isotopic ratio is indistinguishable from the initial $^{87}Sr/^{86}Sr$ ratio (0.7086) of the Capilla del Monte granite in the Sierra de Córdoba (Fig. 1), which is also Early Carboniferous (Rb–Sr isochron age of 337 Ma; Saavedra et al., 1998). This similarity suggests that the magmas for these two plutons came from an isotopically similar source.

New whole-rock Rb–Sr isotope data for the Zapata and Huaco granitic complexes are reported in Table 3a. Analytical details are found in electronic Appendix A. For the Zapata granitic complex, initial ratios at the reference age of 323 Ma range from 0.7098 to 0.7114. A fourth sample (ZAP-27) yielded an anomalous value of 0.6776. Because the reference age is a K–Ar cooling age the initial Sr isotope ratios of the Zapata magmas were probably lower than the values given above. For the Huaco granitic complex, initial ratios at a reference age of 354 Ma for three of the samples range from 0.7044 to 0.7062. Again, a fourth sample (HUA-13) yielded an anomalous initial ratio of 0.6915. The two anomalous samples also show lower Sr contents, probably reflecting perturbation of the Rb–Sr systematics after crystallization by an alteration event. Isochron plots for both sets of samples yield errorchrons. In particular, Söllner et al. (2007) recognized an alteration event in the Huaco granite at 315 ± 42 Ma. Well constrained Sr isotope initial ratios for the Carboniferous granites are highly variable from 0.7044 to 0.7086.

7.2. Sm–Nd isotopes

Nineteen samples from the Los Árboles ($n = 5$) and the San Blas ($n = 4$) plutons, and the Huaco ($n = 5$) and the Zapata ($n = 5$) granitic complexes were analysed for their Nd isotopic composition. Analytical details are found in electronic Appendix A. Epsilon Nd values (ε_{Ndt}) were calculated for the inferred crystallization age (Table 3b).

All samples have roughly similar $^{147}Sm/^{144}Nd$ (0.1090–0.1616) and $^{143}Nd/^{144}Nd$ (0.512234–0.512537) ratios. Ranges of ε_{Ndt} values are: Los Árboles pluton (−0.8 to −2.6, at 335 Ma), San Blas pluton (+0.6 to −4.8; at 340 Ma), Huaco granitic complex (−2.4 to −3.4; at 354 Ma), Zapata granitic complex (−2.6 to −3.9; at 323 Ma) (Table 3b). Except for one sample from the San Blas pluton (SBP-10, $\varepsilon_{Ndt} = +0.6$, Table 3b) all the ε_{Ndt}s are negative and vary between −0.8 and −4.8. Nd model ages calculated according to De Paolo et al. (1991) are between 0.96 and 1.72 Ga, i.e., Proterozoic, with a peak between 1.00 and 1.40 Ga (Table 3b).

Table 3b
Sm–Nd composition of representative samples from the studied granitic rocks.

Samples	SiO_2 (wt.%)	Age (Ma)	Sm	Nd	$^{147}Sm/^{144}Nd$	$(^{143}Nd/^{144}Nd)_{today}$	$(^{143}Nd/^{144}Nd)t$	ε_{Ndt}	T_{DM}^{*}(Ga)
FIA-3	69.21	335	12.1	67.1	0.1090	0.512351	0.512112	−1.8	1.03
FIA-8	70.51	335	11.9	64.0	0.1124	0.512320	0.512073	−2.6	1.10
FIA-17	74.50	335	12.1	51.5	0.1420	0.512434	0.512123	−1.6	1.29
FIA-18	75.30	335	12.5	52.0	0.1453	0.512458	0.512139	−1.3	1.30
FIA-22	72.77	335	11.2	61.7	0.1097	0.512406	0.512165	−0.8	0.96
HUA-4	74.61	354	4.58	20.10	0.1377	0.512338	0.512019	−3.2	1.40
HUA-6	72.79	354	10.2	46.5	0.1326	0.512365	0.512058	−2.4	1.28
HUA-7	72.62	354	9.75	43.6	0.1352	0.512335	0.512022	−3.1	1.37
HUA-12	73.30	354	10.5	49.1	0.1293	0.512352	0.512052	−2.5	1.25
HUA-13	72.39	354	9.24	44.8	0.1247	0.512318	0.512029	−3.0	1.25
SBP-6	75.49	340	17.0	82.1	0.1252	0.512234	0.511955	−4.8	1.38
SBP-9	71.83	340	9.58	47.5	0.1219	0.512395	0.512124	−1.5	1.09
SBP-10	76.01	340	16.8	73.9	0.1374	0.512537	0.512231	0.6	1.04
SBP-15	73.92	340	11.10	59.50	0.1128	0.512365	0.512114	−1.7	1.04
ZAP-26	72.70	323	17.10	92.30	0.1120	0.512258	0.512021	−3.9	1.19
ZAP-27	75.11	323	18.60	69.60	0.1616	0.512430	0.512088	−2.6	1.72
ZAP-29	73.46	323	15.10	64.50	0.1415	0.512366	0.512067	−3.0	1.41
ZAP-33	71.86	323	9.71	46.30	0.1268	0.512306	0.512038	−3.6	1.29
ZAP-35	73.37	323	6.60	33.80	0.1180	0.512297	0.512047	−3.4	1.20

The decay constants used in the calculations are $\lambda^{87}Rb = 1.42 \times 10^{-11}$ and $\lambda^{147}Sm = 6.54 \times 10^{-12}$ year^{-1} recommended by the IUGS Sub-commission for Geochronology (Steiger and Jäger, 1977). Epsilon-Sr (εSr) values were calculated relative to a uniform reservoir present day: $(^{86}Rb/^{87}Sr)_{UR}^{today} = 0.0827$; $(^{87}Sr/^{86}Sr)_{UR}^{today} = 0.7045$. Epsilon Nd ($\varepsilon$Nd) values were calculated relative to a chondrite present day: $(^{143}Nd/^{144}Nd)_{CHUR}^{today} = 0.512638$; $(^{143}Sm/^{144}Nd)_{CHUR}^{today} = 0.1967$.
t = time used for the calculation of the isotopic initial ratios. T_{DM}^{*} = calculated according to De Paolo et al. (1991).
The ages are: FIA-17 (335 Ma, Grissom et al., 1998), HUA-4 (354 Ma, Söllner et al., 2007), SBP-15 (340 Ma, Dahlquist et al., 2006), ZAP (323 Ma, McBride, 1972; McBride et al., 1976).

8. Petrogenetic discussion

The whole-rock geochemical signatures (Figs. 4, 6, 7, 8) and the biotite chemistry (Fig. 9) indicate that these Early Carboniferous granitoids are A-type granitoids. As suggested by Eby (1990, 1992), A-type granites can be formed in a variety of ways. The challenge is to determine which of the possible petrogenetic models applies to a particular occurrence. The proposed petrogenetic models are (i) fractionation of mantle-derived magma, (ii) reaction of mantle-derived magma with crustal rocks, (iii) melting of deep continental crust, and (iv) partial melting of continental crust (metasomatized or not) (Abdel Rahman, 2006; Konopelko et al., 2007). In particular, a petrogenetic model (iv) has been invoked to explain the origin of A-type felsic melts (see Abdel Rahman, 2006 and references therein).

8.1. Source of the granitoid magmas — discrimination diagrams and isotopic data

On the tectonic discriminant diagram of Pearce et al. (1984), the granitic rocks plot in the field of within-plate granite (WPG, Fig. 10a). Eby (1990, 1992) subdivided the A-type granites into two groups: A_1 and A_2, both emplaced in anorogenic settings. It was suggested that the A_1 group was mantle-derived while the A_2 group was derived from melting of continental crust with or without a mantle input. On the Y–Nb–3×Ga (Fig. 10b) discriminant diagram of Eby (1990) the granites plot in the A_2 field which is compatible with a dominantly crustal origin.

The isotopic data for the Early Carboniferous granites (negative ε_{Ndt} values and comparatively moderate to high Sr isotope initial ratios) strongly suggest the involvement of crustal sources in the generation of the magmas that contained Nd extracted from the mantle in the Mesoproterozoic (between 1.0 and 1.4 Ga) (Table 3b). Significant participation of Ordovician meta-granitoids in the source of the Huaco granitic complex was also recognized by Grosse et al. (2009). Consistently, there are A-type granites that postdate spatially associated calc-alkaline rocks and that have isotopic and trace element compositions that suggest derivation from these calc-alkaline precursors (e.g., North America, Anderson, 1983; Egypt, Abdel Rahman, 2006; Kyrgyzstan, Konopelko et al., 2007).

Most of the Early Ordovician granites show T_{DM} ages between 1.5 and 1.7 Ga and Nd isotopic signatures (ε_{Ndt} values between −5 and −6 at the time of crystallization between 490 and 468 Ma) (Dahlquist et al., 2008, and references therein). However, ε_{Ndt}s are less negative (+0.6 to −4.8 at 323 to 354 Ma) compared to values of Famatinian granitoids at the same time (−4.8 to −8.5) (Table 3b and in a supplemental electronic data table). The ε_{Ndt} values for the Early Carboniferous granitoids (Table 3b and supplemental electronic data table) are displaced towards ε_{Ndt} typical of the asthenospheric mantle. Thus, the participation of an asthenospheric component (together with the old lithosphere component) is required to satisfy the ε_{Ndt} values calculated for the Early Carboniferous granitoids. A simple mixing calculation using equation 9.1 of Faure (1986, page 141) and a Nd isotopic asthenospheric mantle signature (CHUR) and Nd isotopic Ordovician granitoids (potential crustal protoliths) data at the time of crystallization of the Carboniferous A-type granites (t = 338 Ma) indicates a dominant asthenospheric participation (63% and 37% of asthenospheric mantle and continental lithosphere, respectively; calculation in Table 4 and isotopic data can be found in a supplemental electronic data table). In fact our interpretation is that the primary magma source was an asthenospheric mantle with subsequent crustal contamination, a hypothesis that is in accord with other works (e.g., Konopelko et al., 2007; Bonin, 2007). In agreement with Bonin (2007), the original concept of A-type granites of Loiselle and Wones (1979) contrasts sharply with the general philosophy of the overall genetic alphabet, where I-, S-, and M-type granites are derived from igneous, sedimentary and mantle source, respectively. A-type granites were defined as anorogenic granites that occur in rift zones and stable continental blocks, without mentioning a particular source. Perhaps the most important point from the abstract of Loiselle and Wones (1979) was that A-type granites have a wide range of isotopic compositions (initial $^{87}Sr/^{86}Sr$ ratios ranging from 0.703 to 0.712), suggesting different mixing proportions of asthenospheric

Table 4
Two-component mixtures using equation 9.1 from Faure (1986, page 141).

(1) $X_M = f_A\,(X_A - X_B) + X_B$
(2) $X_M - X_B = f_A\,(X_A - X_B)$
(3) $X_M - X_B/(X_A - X_B) = f_A$
(4) f_A = 0.63 or 63%.

X_A = Isotopic composition of asthenospheric mantle, $^{143}Nd/^{144}Nd = 0.512203$; X_B = Isotopic compositions of potential crustal protoliths that outcrop in the Sierras Pampeanas: I- and S-type Ordovician granites, $^{143}Nd/^{144}Nd = 0.511867$; X_M = Isotopic assumed mixed composition, represented by Carboniferous A-type granites, $^{143}Nd/^{144}Nd = 0.512078$. f_A = Asthenospheric mantle fraction in the mixture. $^{143}Nd/^{144}Nd$ compositions for X_A, X_B, and X_M, are recalculated to t = 338 Ma, the average of the Carboniferous crystallization ages (Table 3b). Data used in the calculation are available in the isotopic supplemental electronic data table.

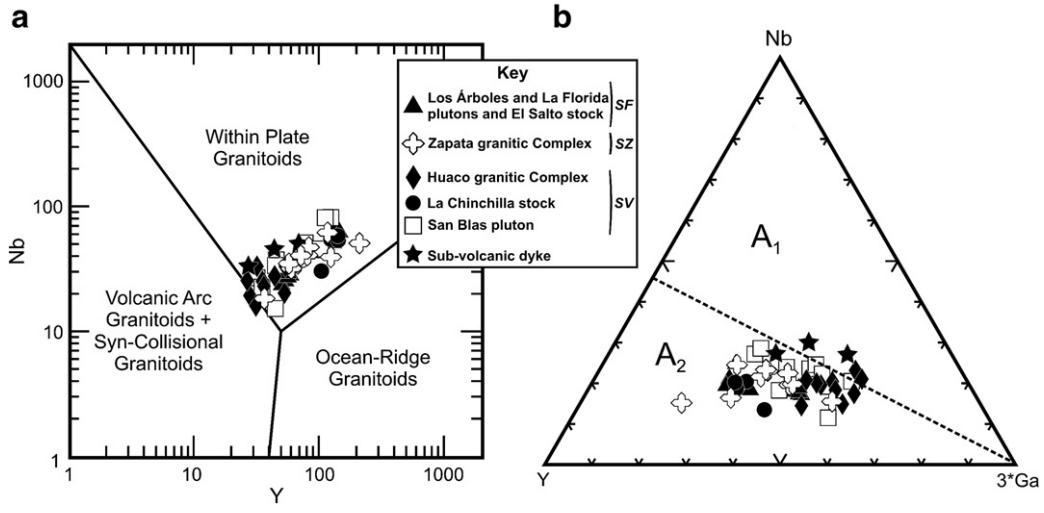

Fig. 10. (a) Tectonic discriminant diagram (Pearce et al., 1984) for the studied granites. The granites plot in the within-plate granite field. (b) Studied granites plotted on the triangular Y–Nb–3×Ga diagram of Eby (1992) used to distinguish between different source rocks for A-type magmas. A_1 field is mantle-derived granites, A_2 field is crustal-derived granites.

mantle and crustal sources. Thus, our main conclusion is that the A-type granites represent variable mixtures of asthenospheric mantle and continental crust, and different mixing ratios lead to the different subtypes of A-type granites (illustrating the lack of consensus about A-type magma origin, Bonin, 2007). The shear zones (see Section 8.3) play an important role, providing suitable conduits for ascending asthenospheric material and heat flux into the crust, a hypothesis that is in accord with the work of Loiselle and Wones (1979) and other recent work about A-type granites (e.g., Abdel Rahman, 2006; Konopelko et al., 2007).

8.2. Petrogenesis of the granitoid magmas

Given that these are metaluminous to peraluminous granitoids, the zircon geothermometer of Watson and Harrison (1983) can be used to estimate magmatic temperatures. The results of these calculations are given in Table 1 for *M* values between 0.9 and 1.7 (the calibration range for the geothermometer). The calculated temperatures (°C) are: Los Árboles Pluton = 831 ± 27 (range = 749 to 857), San Blas pluton = 792 ± 34 (range = 736 to 820), Huaco granitic complex = 779 ± 37 (range = 683 to 835), La Chinchilla stock = 746 ± 18 (range = 720 to 757), and Zapata granitic complex = 803 ± 15 (range = 790 to 833). These are maximum temperatures because the presence of inherited zircon, as identified in the Huaco granitic complex (Söllner et al., 2007), will result in higher calculated temperatures. A crude correlation between the calculated temperature and the Eu anomaly is observed for each pluton or granitic complex. Consistently, the temperature decreases as the Eu anomaly becomes more negative (Table 1) giving confidence to the values obtained using the zircon geothermometer.

Chondrite-normalized REE plots and primitive mantle-normalized spider diagrams (Fig. 8) show several distinctive features. (1) REE patterns tend to be flat to slightly LREE enriched and have significant negative Eu anomalies indicating that feldspar fractionation or residual feldspar in the source region played a role in the petrogenesis of the magmas. (2) Significant negative Ba and Sr anomalies on the spider diagrams similarly support the important role of feldspar (Fig. 11). (3) Significant negative P and Ti anomalies indicate, respectively, that apatite and Fe–Ti oxides also played a role. (4) LIL elements are significantly enriched with respect to primitive mantle. (5) For the element pairs — Zr/Hf and Nb/Ta, Hf is relatively enriched with respect to Zr and Ta is relatively enriched with respect to Nb. This leads to lower Zr/Hf and Nb/Ta ratios, compared to primitive mantle, and values that fall in the range for average crust suggesting that there is a significant crustal component in the melts. There is also a significant variation in the ratios which suggests that there has been some post-intrusion mobility.

Logarithmic plots of Eu versus Ba and Sr concentrations show linear trends for the Los Árboles pluton, San Blas pluton, and Zapata and Huaco granitic complex (Fig. 11). The La Chinchilla stock occurs as small granite body in the Huaco granitic complex (Fig. 2) and represents a late magmatic pulse with a restricted range in composition (Fig. 11). For this reason it is not considered in this analysis. Both Ba and Sr decrease with decreasing Eu (Fig. 11) showing the role of feldspar fractionation in the evolution of these magmas. In the case of perfect fractional crystallization for a particular pluton or complex, the samples will form a linear trend that shows the relative proportions of K-feldspar and plagioclase fractionating from the magma. If this proportion changes as the magma evolves the trend will be curved. Linear trends for a number of the suites indicate that K-feldspar and plagioclase fractionated in an approximately 50:50 ratio (Fig. 11). However, scattering of the data beyond analytical error suggests that the system was not entirely closed and that there was some interaction with the crust. For the Huaco granitic complex the samples plot in a field indicating that fractional crystallization was not important in this case, but that there was residual feldspar in the

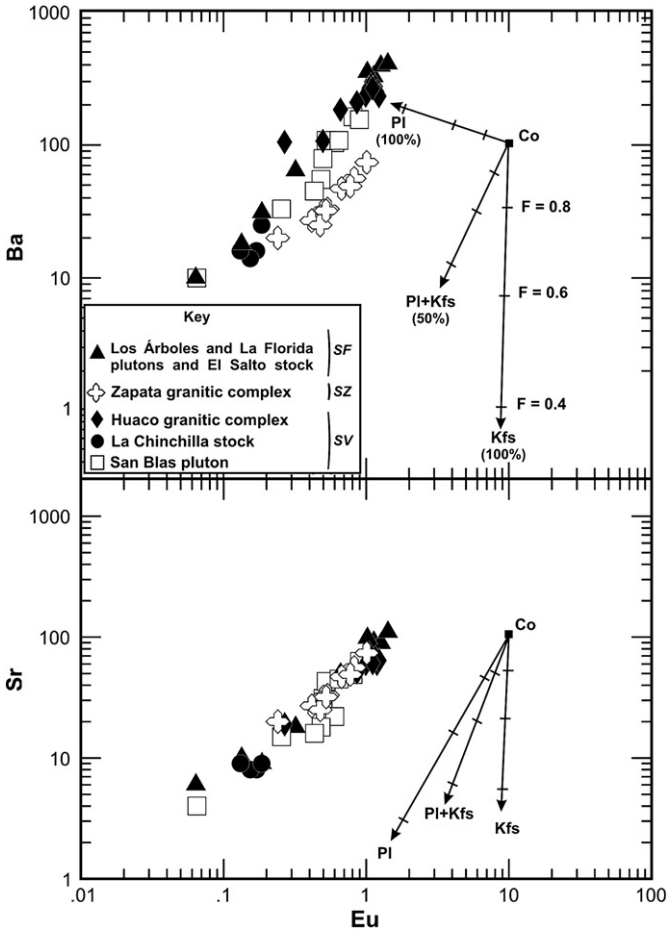

Fig. 11. (a) Ba vs. Eu and (b) Sr vs. Eu. Linear trends for a number of the suites indicate that K-feldspar (Kfs) and plagioclase (Pl) crystallize in an approximately 50:50 ratio. The partition coefficient data for minerals in equilibrium with granitic liquids are from Rollinson (1994, Table 4.3.) and Nagasawa and Schnetzler (1971). The crystallization percentage for Kfs and Pl is indicated in the figure. Co = Initial concentration, F = weight fraction of remaining melt.

source region. Note that for all of the complexes all samples, including the more mafic dikes, show negative Eu anomalies (Fig. 8) which supports the inference that the magmas were initially in equilibrium with a feldspar-containing source region.

The high Ga/Al ratio is a distinctive or typical characteristic of the metaluminous A-type granites, and plots of these ratios against major and trace element data readily distinguish these granites from I-type (calc-alkaline) and S-type granites (Whalen et al., 1987). Thus, using the Ga vs. Ga/Al diagram, metaluminous A-type granites of Early Carboniferous age are distinguished from the calc-alkaline granites crystallized in the Famatinian Orogen of Argentina (Ordovician) and strongly support the A-type signature for the studied granites (Fig. 12). Experimental result by Patiño Douce (1997, 1998) indicate that the higher proportion of Ca-rich plagioclase formed by incongruent melting in low pressure conditions (4 kbar) explains the low CaO relative to Al_2O_3 (Fig. 12) of the metaluminous A-type granites (as well as their Eu depletion) and, because plagioclase excludes Ga relative to Al_2O_3 (Malvin and Drake, 1987), also gives rise to the distinctively high Ga/Al ratios of the metaluminous A-type granites. Therefore, fractional crystallization (with feldspar fractionation) as well as residual feldspar in the source region is the main process invoked for the generation of these A-type granites.

Our data bank containing chemical analysis of biotite minerals from calc-alkaline magmas (I- and S-type) and granites of A-type signature in the proto-Andean margin indicates that biotite composition depends largely upon the nature of magma as was originally

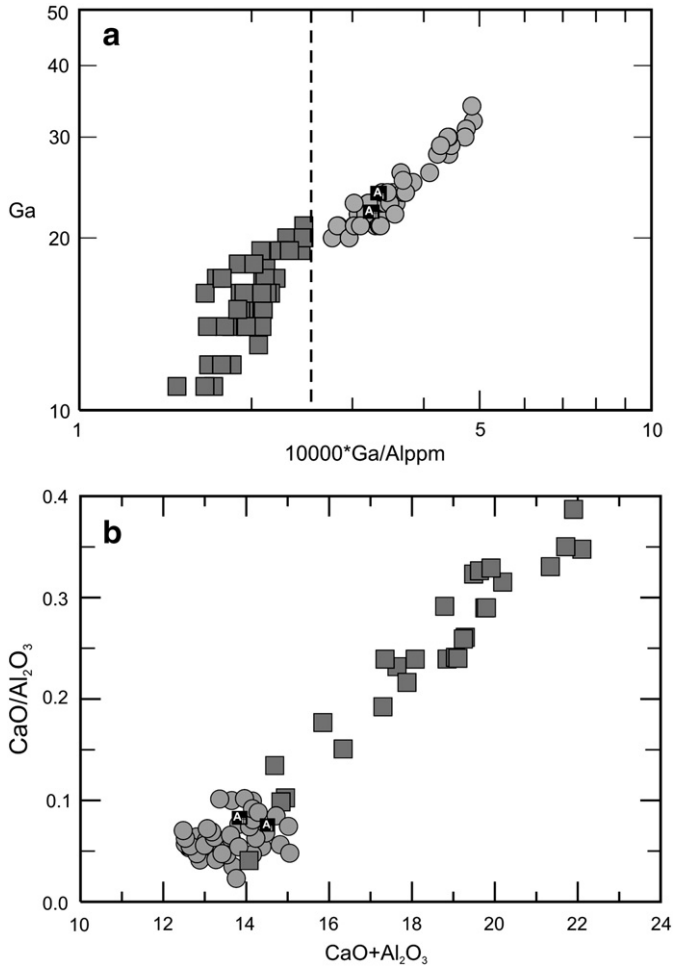

Fig. 12. Al_2O_3, CaO, and Ga diagrams showing the compositions of the studied A-type granites (filled circle) and the Famatinian calc-alkaline granitoids (filled square). For the Famatinian calc-alkaline granitoids the SiO_2 content ranges from tonalites (SiO_2 = 60 wt.%) to monzogranites (SiO_2 = 75 wt.%). Chemical data for the Famatinian granitoids are from Dahlquist et al. (2005b, 2008). The 10,000 × Ga/Al discrimination limit for A-type granites is from Whalen et al. (1987). A_i and A_{ii} are A-type average composition from Konopelko et al. (2007) and Chappell and White (1992), respectively.

suggested by Abdel Rahman (1994). Biotite minerals define three compositionally distinct fields in the MgO vs. FeO discriminatory diagram of Abdel Rahman (1994). Biotites in the A-type granites here studied are iron-rich while biotites in calc-alkaline rocks (I- and S-type granites) are moderately enriched in MgO (Fig. 9).

The calculated magma F and Cl content (together with the mg #) for these A-type granitoids (F = 580–5600 ppm and Cl = 90–1180 ppm, see Section 5) is generally higher than that for calc-alkaline granites (F = 0–470 ppm and Cl = 0–250 ppm) although the values are not excessively high, i.e., water is still a significant part of the volatile component of the magmas. Thus, F and Cl content of igneous biotites seem to reflect the nature of their parental host magmas and are potential chemical elements to be used in discriminant diagrams.

8.3. The thermal source for continental lithosphere anatexis

As pointed out by Brown (1994), the heat necessary for crustal anatexis may be the result of internal radiogenic heat production in over-thickened crust, intraplating/underplating of mantle-derived magma, an enhanced flux from the mantle, or some combination of these mechanisms. Moreover, Black et al. (1984) showed that large faults play a major role during the emplacement of alkaline felsic magmas, as do transform faults whose position may well have been determined by older lineaments in the continents. The role of intra-continental shear zones and fault systems in the generation, ascent and emplacement of granitic magmas has also been emphasized by Brown (1994) and Abdel Rahman (2006). The Early Carboniferous granitic plutons considered here are related to the prominent TIPA shear zone that underwent heating coeval to Early Carboniferous magmatism. Although the history of this shear zone deserves further research, and normal and reverse sense of movement have been proposed (Grissom et al., 1998; Höckenreiner et al., 2003), we infer that the TIPA shear zone was active in the Early Carboniferous and could have controlled the emplacement of plutons. Melting of continental crust was probably triggered by mantle-derived magmas as inferred from isotope evidence given previously. Subsequent ascent of granitic magma was focused along the TIPA shear zone. Heat advected to the upper crust by rising magmas favoured ductile deformation and recrystallization (~342–328 Ma) within the shear zone. Cooling continued long after pluton emplacement (~300 Ma).

9. Conclusions

The whole-rock chemical and geochronological data allow us to determine unequivocally that these plutons are A-type granites emplaced during the Early Carboniferous in the proto-Andean margin of Gondwana. The main conclusions of this study, which could be applicable to other A-type granites, are:

(1) A-type magmas represent variable mixtures of asthenospheric mantle and continental crust, and variations in the mixing ratios lead to different subtypes of A-type granite. In our study the magma source was primarily (and dominantly) mantle with subsequent crustal contamination.
(2) Shear zones (in our study the TIPA shear zone) play an important role, providing suitable conduits for ascending asthenospheric material and heat flux into the crust, a hypothesis that is in accord with other recent work about A-type granites.
(3) Biotites have distinctive compositions with high FeO/MgO ratios, F, and Cl. Thus, FeO/MgO ratios together with F and Cl content of igneous biotites seem to reflect the nature of their parental host magmas and may be useful in identifying A-type granitoids.
(4) Our petrogenetic model supports progressive fractional crystallization with dominant fractionation of feldspar and a source mineral assemblage enriched in plagioclase, explaining the distinctive negative Eu anomalies observed in A-type granites.

Acknowledgements

Financial support was provided by the Yacimientos Minerales Riojanos (YAMIRI S.A.), SECyT UNLaR grants Exp. No. 6977/07, and by the Spanish MEC grants CGL2005-02065/BTE. Dr. Norman Charnley, Oxford, assisted with the electron microprobe analyses of the San Blas pluton biotites. The careful and thorough reviews by two anonymous journal reviewers contributed significantly to the final form of the manuscript. We thank Andrew Kerr for his editorial handling of the manuscript.

Appendix A. Supplementary data

Supplementary data associated with this article can be found, in the online version, at doi:10.1016/j.lithos.2009.11.006.

References

Abdel Rahman, A.M., 1994. Nature of biotites from alkaline, calc-alkaline, and peraluminous magmas. Journal of Petrology 35, 525–541.
Abdel Rahman, A.M., 2006. Petrogenesis of anorogenic peralkaline granitic complexes from eastern Egypt. Mineralogical Magazine 70, 27–50.

Aceñolaza, F.G., Miller, H., Toselli, A.J., 2000. Geología de la Sierra de Velasco, Provincia de La Rioja, Argentina. Geowissenscallliches Lateinamerika-Kolloquium. Profil, Band 18. Extended Abstracts in CD-ROM. Stuttgart. In Spanish.

Alasino, P.H., 2002. Caracterización Petrológica del sector NE de la Sierra de Velasco, La Rioja, Argentina. Undergraduate thesis, Universidad Nacional de Córdoba, Argentina (In Spanish).

Alasino, P.H., 2007. Geología, petrología y geoquímica de los granitoides Famatinianos ubicados en el sector occidental, y su comparación con el sector central, a los 29° de latitud sur del margen proto-andino de Gondwana, Sierras Pampeanas, Argentina. Ph.D., Universidad Nacional de Córdoba, Argentina (In Spanish).

Alba, F., 2008. Caracterización petrológica y geoquímica del plutón San Blas, provincia de La Rioja, Argentina. Undergraduate thesis. Universidad Nacional de San Juan, Argentina (In Spanish).

Anderson, J.L., 1983. Proterozoic anorogenic granite plutonism of North America. Proterozoic Geology, Selected Papers from an International Proterozoic Symposium: In: Mederis, L.G., Byers, C.W., Mickelson, D.M., Shanks, W.C. (Eds.), Geological Society of America Memoir, vol. 161, pp. 133–152.

Báez, M.A., Rossi de Toselli, J., Sardi, F., 2002. Consideraciones preliminares sobre los granitoides del norte de la Sierra de Velasco, La Rioja, Argentina. In: Cabaleri, N., Cingolani, C., Linares, E., López de Luchi, M., Ostera, H., Panarello, H. (Eds.), Actas del XV Congreso Geológico Argentino, vol. 2, pp. 69–74 (In Spanish).

Báez, M.A., Basei, M.A., Toselli, A.J., Rossi, J.N., 2004. Geocronología de granitos de la sierra de Velasco (Argentina): reinterpretación de la secuencia magmática. Actas Simposio 40 años de geocronología en Brasil, San Pablo, Brasil, p. 85 (In Spanish).

Black, R., Lameyre, J., Bonin, B., 1984. The structural setting of alkaline complexes. Journal of African Earth Sciences 3, 5–16.

Bonin, B., 2007. A-type granites and related rocks: evolution of a concept, problems and prospects. Lithos 97, 1–29.

Boynton, W.V., 1984. Geochemistry of the rare earth elements: meteorites studies. In: Henderson, P. (Ed.), Rare Earth Element Geochemistry. Elsevier. 63–114 pp.

Brown, M., 1994. The generation, segregation, ascent and emplacement of granite magma: the migmatite-to-crustally-derived granite connection in thickened orogens. Earth-Science Reviews 36, 83–130.

Büttner, S.H., Glodny, J., Lucassen, F., Wemmer, K., Erdmann, S., Handler, R., Franz, G., 2005. Ordovician metamorphism and plutonism in the Sierra de Quilmes metamorphic complex: implications for the tectonic setting of the northern Sierras Pampeanas (NW Argentina). Lithos 83, 143–181.

Chappell, B.W., White, A.J.R., 1992. I- and S- type granites in the Lachlan Fold Belt. Transactions of the Royal Society of Edinburgh: Earth Sciences 83, 1–26.

Dahlquist, J.A., Galindo, C., 2004. Geoquímica isotópica de los granitoides de la sierra de Chepes: un modelo geotectónico y termal, implicancias para el orógeno famatiniano. Revista de la Asociación Geológica Argentina 59, 57–69 (In Spanish).

Dahlquist, J.A., Rapela, C.W., Pankhurst, R.J., Baldo, E., Saavedra, J., Alasino, P.H., 2005b. Los granitoides de la sierra de Chepes y su comparación con granitoides paleozoicos de las Sierras Pampeanas: implicancias para el orógeno famatiniano. Geología de la provincia de La Rioja — Precámbrico–Paleozoico Inferior: In: Dahlquist, J.A., Baldo, E.G., Alasino, P.H. (Eds.), Asociación Geológica Argentina, Serie D, Publicación Especial, vol. 8, pp. 87–108 (In Spanish).

Dahlquist, J.A., Rapela, C.W., Baldo, E., 2005a. Petrogenesis of cordierite-bearing S-type granitoids in Sierra de Chepes, Famatinian orogen, Argentina. Journal of South American Earth Sciences 20, 231–251.

Dahlquist, J.A., Pankhurst, R.J., Rapela, C.W., Casquet, C., Fanning, C.M., Alasino, P., Baez, M., 2006. The San Blas Pluton: an example of Carboniferous plutonism in the Sierras Pampeanas, Argentina. Journal of South American Earth Sciences 20, 341–350.

Dahlquist, J., Casquet, C., Alasino, P., Galindo, C., Grant, C., Medina, C., 2007. A-type granitoids in the Eastern Sierras Pampeanas (Argentina): evidence for early carboniferous aborted rifting? GEOSUR, An International Congress on the Geology and Geophysics of Southern Hemisphere Abstracts Volume, p. 47.

Dahlquist, J.A., Pankhurst, R.J., Rapela, C.W., Galindo, C., Alasino, P., Fanning, C.M., Saavedra, J., Baldo, E., 2008. New SHRIMP U–Pb data from the Famatina complex: constraining Early–Mid Ordovician Famatinian magmatism in the Sierras Pampeanas, Argentina. Geologica Acta 6, 319–333.

De Paolo, D.J., Linn, A.M., Schubert, G., 1991. The continental crustal age distribution: methods of determining mantle separation ages from Sm–Nd isotopic data and application to the Southwestern United States. Journal of Geophysical Research 96, 2071–2088.

Dorais, M.J., Lira, R., Chen, Y., Tingey, D., 1997. Origin of biotite–apatite-rich enclaves, Achala batholith, Argentina. Contributions to Mineralogy and Petrology 130, 31–46.

Eby, G.N., 1990. The A-type granitoids: a review of their occurrence and chemical characteristics and speculations on their petrogenesis. Lithos 26, 115–134.

Eby, G.N., 1992. Chemical subdivision of the A-type granitoids: petrogenetic and tectonic implications. Geology 20, 641–644.

Faure, G., 1986. Principles of isotope geology, Second Edition. John Wiley & Sons. 589 pp.

Frost, B.R., Barnes, C.G., Collins, W.J., Arculus, R.J., Ellis, D.J., Frost, C.D., 2001. A geochemical classification for granitic rocks. Journal of Petrology 42, 2033–2048.

Grissom, G.C., Debari, S.M., Lawrence, W.S., 1998. Geology of the Sierra de Fiambala, northwestern Argentina: implications for early Palaezoic Andean tectonics. In: Pankhurst, R.J., Rapela, C.W. (Eds.), The Proto-Andean Margin of Gondwana. Geological Society, London, Special Publications, vol. 142, pp. 297–323.

Grosse, P., Söllner, F., Baéz, M.A., Toselli, A.J., Rossi, J.N., de la Rosa, J.D., 2009. Lower Carboniferous post-orogenic granites in central-eastern Sierra de Velasco, Sierras Pampeanas, Argentina: U–Pb monazite geochronology and Sr–Nd isotopes. International Journal of Earth Science 98, 1001–1025.

Höckenreiner, M., Söllner, F., Miller, H., 2003. Dating the TIPA shear zone: an early Devonian terrane boundary between the Famatinian and Pampean systems (NW Argentina). Journal of South America Earth Sciences 16, 45–66.

Icenhower, J., London, D., 1997. Partitioning of fluorine and chlorine between biotite and granitic melt: experimental calibration at 200 MPa H_2O. Contributions to Mineralogy and Petrology 127, 17–29.

Konopelko, D., Biske, G., Seltmann, R., Eklund, O., Belyatsky, B., 2007. Hercynian post-collisional A-type granites of the Kokshaal Range, Southern Tien Shan, Kyrgyzstan. Lithos 97, 140–160.

Kretz, R., 1983. Symbols for rock-forming minerals. American Mineralogist 68, 277–279.

Llambías, E.J., Sato, A.M., Ortiz Suárez, A., Prozzi, C., 1998. The granitoids of the Sierra de San Luis. The Proto-Andean margin of Gondwana: In: Pankhurst, R.J., Rapela, C.W. (Eds.), Geological Society of London, Special Publication, vol. 142, pp. 325–341.

Loiselle, M.C., Wones, D.R., 1979. Characteristics and origin of anorogenic granites. Abstracts of papers to be presented at the Annual Meetings of the Geological Society of America and Associated Societies, San Diego, California, November 5–8, vol. 11, p. 468.

López de Luchi, M.G., Siegesmund, S., Wemmer, K., Steenken, A., Naumann, R., 2007. Geochemical constraints on the petrogenesis of the Paleozoic granitoids of the Sierra de San Luis, Sierras Pampeanas, Argentina. Journal of South American Earth Science 24, 138–166.

Malvin, D.J., Drake, M.J., 1987. Experimental determination of crystal/melt partitioning of Ga and Ge in the system forsterite–anorthite–diopside. Geochemica et Cosmochimica Acta 51, 2117–2128.

McBride, S.L., 1972. A Potassium–argon age investigation of igneous and metamorphic rocks from Catamarca and La Rioja provinces, Argentine. PhD. Thesis. Queen's University (unpublished). Ontario. Canada.

McBride, S.L., Caelles, J.C., Clark, A.H., Farrar, E., 1976. Paleozoic radiometric age provinces in the Andean basement, latitudes 25°–30°S. Earth and Planetary Science Letters 29, 373–383.

Miller, H., Söllner, F., 2005. The Famatina complex (NW-Argentina): back-docking of an island arc or terrane accretion? Early Palaeozoic geodynamics at the western Gondwana margin. In: Vaughan, A.P.M., Leat, P.T., Pankhurst, R.J. (Eds.), Terrane processes at the margins of Gondwana. Geological Society of London, Special Publication, vol. 246, pp. 241–256.

Miller, C.F., McDowell, S.M., Mapes, R.W., 2003. Hot and cold granites? Implications of zircon saturation temperatures and preservation of inheritance. Geology 31, 529–532.

Miyashiro, A., 1978. Nature of alcalic volcanic rock series. Contributions to Mineralogy and Petrology 66, 91–104.

Muñoz, J.L., 1984. F–OH and Cl–OH exchange in micas with applications to hydrothermal ore deposits. In: Bailey, S.W. (Ed.), Reviews in Mineralogy, Micas, vol. 13. Mineralogical Society of America, pp. 469–493.

Muñoz, J.L., 1992. Calculation of HF and HCl fugacities from biotite compositions: revised equations. Geological Society of America, Abstracts with Programs 24, A221.

Nagasawa, H., Schnetzler, C.C., 1971. Partitioning of rare Earth, alkali, and alkaline Earth elements between phenocrysts and acidic igneous magmas. Geochimica et Cosmochimica Acta 35, 953–968.

Nakamura, N., 1974. Determination of REE, Ba, Mg, Na and K in carbonaceous and ordinary chondrites. Geochimica et Cosmochimica Acta 38, 757–773.

Pankhurst, R.J., Rapela, C.W., Saavedra, J., Baldo, E.G., Dahlquist, J.A., Pascua, I., Fanning, C.M., 1998. The Famatinian arc in the central Sierras Pampeanas: an early to mid-Ordovician continental arc on the Gondwana margin. The Proto-Andean Margin of Gondwana: In: Pankhurst, R.J., Rapela, C.W. (Eds.), Geological Society, London, Special Publications, vol. 142, pp. 343–367.

Pankhurst, R.J., Rapela, C.W., Fanning, C.M., 2000. Age and origin of coeval TTG, I–S-type granites in the Famatinian belt of NW Argentina. Transactions of the Royal Society of Edinburgh, Earth Sciences 91, 151–168.

Patiño Douce, A.E., 1997. Generation of metaluminous A-type granites by low-pressure melting of calc-alkaline granitoids. Geology 25, 743–746.

Patiño Douce, A.E., 1998. What do experiments tell us about the relative contributions of crust and mantle to the origin of granitic magmas? Understanding Granites: Integrating New and Classical Techniques: In: Castro, A., Fernández, C., Vigneresse, J.L. (Eds.), Geological Society of London, Special Publications, vol. 168, pp. 55–75.

Pearce, J.A., Harris, N.B.W., Tindle, A.G., 1984. Trace element discrimination diagrams for the tectonic interpretation of granitic rocks. Journal of Petrology 25, 956–983.

Pinotti, L.P., Coniglio, J.E., Esparza, A.M., D'Eramo, F.J., Llambías, E.J., 2002. Nearly circular plutons emplaced by stoping at shallow crustal levels, Cerro Aspero batholith, Sierras Pampeanas de Córdoba, Argentina. Journal of South American Earth Sciences 15, 251–265.

Pinotti, L., Tubía, J.M., D'Eramo, F., Vegas, N., Sato, A.M., Coniglio, J., Aranguren, A., 2006. Structural interplay between plutons during the construction of a batholith (Cerro Aspero batholith, Sierras de Córdoba, Argentina). Journal of Structural Geology 28, 834–849.

Rapela, C.W., Pankhurst, R.J., 1998. The proto-Andean margin of Gondwana: an introduction. The proto-Andean margin of Gondwana: In: Pankhurst, R.J., Rapela, C.W. (Eds.), Geological Society, London, Special Publications, vol. 142, pp. 1–9.

Rapela, C.W., Pankhurst, R.J., Casquet, C., Baldo, E., Saavedra, J., Galindo, C., 1998. Early evolution of the proto-Andean margin of South America. Geology 26, 707–710.

Rapela, C.W., Pankhurst, R.J., Casquet, C., Fanning, C.M., Baldo, E., González-Casado, J.M., Galindo, C., Dahlquist, A., 2007. The Río de la Plata craton and the assembly of SW Gondwana. Earth-Science Reviews 83, 49–82.

Rapela, C.W., Baldo, E.G., Pankhurst, R.J., Fanning, C.M., 2008. The Devonian Achala batholith in the Sierras Pampeanas: F-rich aluminous A-type granites. VI South American Symposium on Isotope Geology, Proceedings in CD-ROM, Paper 53. San Carlos de Bariloche, Argentina.

Rapela, C.W., Pankhurst, R.J., Casquet, C., Baldo, E., Galindo, C., Fanning, C.M., Dahlquist, J.A., in press. Grenville-age magmatism of the Western Sierras Pampeanas,

southern South America: U–Pb SHRIMP dating and tectonic affinities. Journal of South American Earth Sciences. doi:10.1016/j.jsames.2009.08.004.
Rollinson, H.R., 1994. Using geochemical data: evaluation, presentation, interpretation. Longman Scientific & Technical Editions, Singapore. 352 pp.
Saavedra, J., Baldo, E., Pankhurst, R.J., Rapela, C.W., Murra, J., 1998. El granito Capilla del Monte (Sierras Pampeanas de Córdoba, Argentina): edad, geoquímica, génesis y especialización metalogénica. 10 Congreso Latinoamericano de Geología. Actas, vol. 2, p. 372 (In Spanish).
Scheepers, R., 2000. Granites of the Saldania mobile belt, South Africa: radioelements and P as discriminators applied to metallogeny. Journal of Geochemical Exploration 68, 69–86.
Shand, S.J., 1927. The eruptive rocks. John Wiley, New York. 360 pp.
Siegesmund, S., Steenken, A., López de Luchi, M.G., Wemmer, K., Hoffmann, A., Mosch, S., 2004. The Las Chacras–Potrerillos batholith (Pampean Ranges, Argentina): structural evidence, emplacement and timing of the intrusion. International Journal Earth Sciences 93, 23–43.
Sims, J.P., Ireland, T.R., Camacho, A., Lyons, P., Pieters, P.E., Skirrow, R.G., Stuart-Smith, P.G., 1998. U–Pb, Th–Pb and Ar–Ar geochronology from the southern Sierras Pampeanas, Argentina: implications for the Palaeozoic tectonic evolution of the western Gondwana margin. In: Pankhurst, R.J., Rapela, C.W. (Eds.), The Proto-Andean Margin of Gondwana, Geological Society of London, Special Publication, vol. 142, pp. 259–281.
Söllner, F., Gerdes, A., Grosse, P., Toselli, A.J., 2007. U–Pb age determinations by LAICP-MS on zircons of the Huaco granite, Sierra de Velasco (NW–Argentina): a long term history of melt activity within an igneous body. Proc XX Colloquium Latin America Earth Sciences, vol. 1, pp. 57–58. Kiel, Germany.
Steiger, R.H., Jäger, E., 1977. Subcommission of geochronology: convention on the use of decay constants in geo- and cosmochronology. Earth and Planetary Science Letters 36, 359–362.
Streckeisen, A., 1976. To each plutonic rock its proper name. Earth Science Reviews 12, 1–33.
Stuart-Smith, P.G., Camacho, A., Sims, J.P., Skirrow, R.G., Pieters, P.E., Black, L.P., Miró, R., 1999. U–Pb, Th–Pb and Ar–Ar geochronology from the southern, 1999. Uranium–Lead dating of felsic magmatic cycles in the southern Sierras Pampeanas, Argentina: implications for the tectonic development of the proto-Andean Gondwana margin. Laurentia Gondwana connections before Pangea: In: Ramos, V.A., Keppe, I.D. (Eds.), Geological Society of America, Special Paper, vol. 336, pp. 87–114.
Sun, S.S., McDonough, W.F., 1989. Chemical and isotopic systematics of oceanic basalts; implications for mantle composition and processes. Magmatism in the ocean basins: In: Saunders, A.D., Norry, M.J. (Eds.), Geological Society of London, vol. 42, pp. 313–345.
Toselli, G.A., Saavedra, J., Córdoba, G., Medina, 1992. Los granitos peraluminosos de las sierras de Vinquis, Cerro Negro, y Zapata (Sierras Pampeanas), provincia de Catamarca, Argentina. Estudios Geológicos 48, 247–256.
Watson, E.B., Harrison, T.M., 1983. Zircon saturation revisited: temperature and composition effects in a variety of crustal magma types. Earth and Planetary Science Letters 64, 295–304.
Whalen, J.B., Currie, K.L., Chappell, B.W., 1987. A-type granites: geochemical characteristics, discrimination and petrogenesis. Contributions to Mineralogy and Petrology 95, 407–419.
Wilson, M., 1989. Igneous Petrogenesis: A Global Tectonic Approach. Chapman & Hall, London. 446 pp.